Annals of Biomedical Engineering, Vol. 37, No. 12, December 2009 *(© 2009)* pp. 2583–2605
DOI: 10.1007/s10439-009-9801-3

Surgical and Morphological Factors that Affect Internal Mechanical Loads in Soft Tissues of the Transtibial Residuum

S. Portnoy,[1] I. Siev-Ner,[2] Z. Yizhar,[3] A. Kristal,[2] N. Shabshin,[4] and A. Gefen[1]

[1]Department of Biomedical Engineering, Faculty of Engineering, Tel Aviv University, Tel Aviv 69978, Israel; [2]Department of Orthopaedic Rehabilitation, Chaim Sheba Medical Center, Tel Hashomer, Israel; [3]Department of Physical Therapy, Faculty of Medicine, Tel Aviv University, Tel Aviv, Israel; and [4]Department of Diagnostic Imaging, Chaim Sheba Medical Center, Tel Hashomer, Israel

(Received 27 February 2009; accepted 10 September 2009; published online 19 September 2009)

Abstract—The residual limb of transtibial amputation (TTA) prosthetic users is threatened daily by pressure ulcers (PU) and deep tissue injury (DTI) caused mainly by sustained mechanical strains and stresses. Several risk factors dominate the extent of internal tissue loads in the residuum. In this study, we developed a set of three-dimensional finite element (FE) models that were variants of a patient-specific FE model, built from magnetic resonance imaging scans. The set of FE modes was utilized to assess the impact of the following risk factors on the strain/stress distribution in the muscle flap: (i) the tibial length, (ii) the tibial bevelment, (iii) a fibular osteophyte, (iv) the mechanical properties of the muscle, and (v) scarring in different locations and depths. A total of 12 nonlinear FE model configurations, representing variations in these factors, were built and solved. We present herein calculations of compression, tension and shear strains and stresses, von Mises stresses, and strain energy density averaged in critical locations in the muscle flap as well as volumes of concentration of elevated stresses in these areas. Our results overall show higher stresses accumulating in the bone proximity rather than in outlying soft tissues. The longer bone configurations spread the loads toward the external surfaces of the muscle flap. When shortening the truncated bones from 11.2 to 9.2 cm, the von Mises stresses at the distal edges of the bones were relieved considerably (by up to 80%), which indicates a predicted decreased risk for DTI. Decreasing the tibial bevelment mildly, from 52.3° to 37.7° caused propagation of internal stresses from the bone proximity toward the more superficial soft tissues of the residuum, thereby also theoretically reducing the risk for DTI. An osteophyte at the distal fibular end increased the strain and stress distributions directly under the fibula but had little effect (<1%) on stresses at other sites, e.g., under the tibia. Elevation of muscle stiffness (instantaneous shear modulus increase from 8.5 to 16.2 kPa), simulating variation between patients, and muscle flap contraction or spasm, showed the most substantial effect by an acute rise of the von Mises stresses at the bone proximity. The mean von Mises stresses at the bone proximity were approximately twofold higher in the contracted/spastic muscle when compared to the flaccid muscle. Locating a surgical scar in different sites and depths of the residuum had the least influence on the overall loading of the muscle flap (where stresses changed by <7%). Pending further validation by epidemiological PU and DTI risk factor studies, the conclusions of this study can be incorporated as guidelines for TTA surgeons, physical therapists, prosthetists, and the TTA patients themselves to minimize the onset of PU and DTI in this population. Additionally, the present analyses can be used to guide or focus epidemiological research of PU and DTI risk factors in the TTA population.

Keywords—Deep tissue injury, Pressure ulcer, Prosthesis, Patient-specific finite element model, Rehabilitation, Post-amputation.

NOMENCLATURE

3D	Three dimensional
BPL	Bone proximity layer
DTI	Deep tissue injury
FE	Finite element
FPL	Fat proximity layer
MRI	Magnetic resonance imaging
PU	Pressure ulcer
SED	Strain energy density
TTA	Transtibial amputation
VOI	Volume of interest

INTRODUCTION

Transtibial amputation (TTA) patients face ongoing morphological changes of their residual limb.[45] The volume of the residuum stabilizes several months post-amputation.[19] Regrettably, this alleged stability does not last long. The volume of the residuum changes due to weight gain or weight loss,[38] edema,[46] and muscle

Address correspondence to A. Gefen, Department of Biomedical Engineering, Faculty of Engineering, Tel Aviv University, Tel Aviv 69978, Israel. Electronic mail: gefen@eng.tau.ac.il

atrophy.[36] Consequently, the TTA prosthetic user is fitted with a new prosthetic socket approximately every 4 years. Despite new innovations in socket and liner materials and design, contemporary prostheses are not yet equipped to confront these changes. The TTA residual limb is therefore subjected to varying superficial and internal mechanical stresses in its soft tissues[41] which—if exceeding critical levels and exposure times—may cause injury.

In addition to the ongoing changes in the volume and shape of the residual limb, the superficial and internal tissue loads in the residuum are affected by the initial geometry of the truncated shinbones, the tibia, and the fibula, which are shaped during the amputation surgery. The post surgery geometry of the bones could also change as the distal bone ends, primarily of the fibula, may develop a spike-like heterotopic ossification, called an osteophyte, if the edges are not covered properly during TTA with the resected periosteum.[13] The primary surgical variants in TTA are the length of the truncated shinbones, the bevelment of the distal end of the tibia, and also the location of the surgical incision which is eventually scarred.[5] The length of the residuum, in particular, was shown to substantially affect limb–socket interface stresses, gait stability,[42] and symmetry.[4] Considering that TTA surgeries are almost as old as the art of surgery,[49] it is extremely surprising that there are no explicit evidence-based guidelines as to the optimal surgical technique for TTA. Rather than methodological scientific studies, there are some rules of thumb, based on clinical experience, which were suggested in the literature over the last decade. For example, surgeons are encouraged to truncate the bones at the most distal site possible.[43] This location is determined by the viability of the soft tissues, evaluated by means of Doppler flowmetry, skin temperature, or segmental blood pressure.[5] There is some controversy regarding the placement of the surgical incision. Pinzur *et al.*[30] suggested that placing the incision directly over the anterior aspect of the distal truncated tibia can potentially produce an adherent scarring of the skin to underlying tissues[31] or insufficient cushioning of this region during load-bearing. Burgess[5] argues that the location of the incision is relatively unimportant. Guidelines for the distal tibial end bevelment are also obscure. In Schwartz's "Principles of Surgery,"[43] the authors suggested bevelment of approximately 45°. Randon *et al.*[35] recommended tibial bevelment up to 60°. Neither claims are scientifically justified.

These discrepancies cause a wide range of residuum shapes across surgeons and medical centers, which are also dictated by the circumstances leading to the TTA (e.g., trauma vs. diabetic limb amputation), as well as the physical condition and co-morbidities of the patient. The literature overall indicates that the immense variability between the external/internal residuum shapes of TTA patients can be characterized by the following key factors[5]: (i) The lengths of the truncated bones, determined in the operation room, (ii) The bevelment (plane of inclination) shaped during operation for the distal tibial end (the fibula is shortened usually 2 cm above the tibial end and the fibular ends are rounded by the surgeon as a standard practice), (iii) Possible development of an osteophyte at the fibula post operation, (iv) Stiffness of the muscle flap, and (v) The location and depth of the surgical scar.

It is important to clarify that variability in muscle flap stiffnesses across TTA patients is not only constituted by the individual tissue mechanical properties but also by the individual neuromuscular interactions in the residuum. For instance, a contractile muscle flap experiences episodes of stiffening during load bearing as the musculature of the limb contracts,[14] whereas a severed muscle flap degenerates and becomes less contractible,[17] more fibrotic or even flaccid.

The five biomechanical factors listed above may considerably affect not only the internal mechanical loads in the soft tissues surrounding the bones, primarily the muscle flap, but also the overlying adipose and skin tissues. Hence, we hypothesize that when some of these biomechanical factors are improperly adjusted, e.g., during surgery (where geometry can, in part, be controlled), or as a result of a post-operative pathobiological process (such as muscle atrophy, osteophytes, or scarring) the consequence can be that some soft tissue regions are overloaded. Such overloading may, over time, risk the wellbeing of the TTA residuum, and of the patient, e.g., by leading to pressure ulcers (PU).[6] The effect of each of these factors on the internal mechanical conditions in the TTA residuum was never investigated before.

Our aim was therefore to obtain data on strains and stress distributions in the soft tissues of the TTA residuum as function of variations in each of the above-listed biomechanical factors, in order to identify the individual factor contributions, which could help in guiding surgeons to shape a more biomechanically optimized residuum. It is important to emphasize that this study is distinguished from all previous literature, since, for the first time, we investigate herein effects on internal soft tissue loads, as opposed to residuum–prosthesis interface pressure or shear[41,50] or gait characteristic.[23,41] This is primarily motivated by the increasing understanding, which is supported by strong, new clinical, and basic research evidence, that TTA patients are susceptible to deep tissue injury (DTI)—a potentially lethal type of PU, where soft tissues subjected to sustained large strains/stresses are necrosing under intact skin.[1,2,13,37] In the TTA

residuum anatomy, the muscle flap tissues are the most susceptible ones to DTI, because of the high sustained loads formed in these tissues that are being deformed directly by the edges of the truncated bones.[33,34] It is particularly important to prevent DTI in TTA patients by appropriately shaping the residual limb, because of the nature of DTI, which onsets in the deep muscle flap tissues, and cannot be detected by conventional interface pressure measurements[40,44,50] or skin temperature mapping.[28]

The contribution of each biomechanical factor, that is, bone length, tibial end bevelment, osteophyte, stiffness of the muscle flap, and scarring were hence tested in a realistic, three-dimensional (3D) finite element (FE) model of a TTA residuum, as further described.

METHODS

In a recent study,[34] we introduced a method for quantifying the state of internal tissue strains and stresses in the TTA residuum. The method is based on integration of a magnetic resonance imaging (MRI) scan of the load bearing residuum during standing together with interface pressure measurements around the residuum, which are then used to develop a patient-specific FE residuum model. This method, described in brief in this article for completeness and depicted in Fig. 1, was applied to build the FE model presented herein.

Characterizing the 3D Anatomy of the Residuum

A traumatic active TTA male prosthetic user (age 44 years, weight 82 kg, 14 years post-amputation) was recruited for this study. Helsinki approval (#4302/06 from Sheba Medical Center, Ramat-Gan, Israel) and informed consent were obtained before the trial. The MRI studies were carried out using an open-MRI (“Signa SP” model, General Electric Co., Fairfield, CT, USA). Images were T1-weighted, which provides maximal contrast between fat tissue (high intensity signal) and skeletal muscle (lower signal intensity), and is therefore optimal for demonstrating anatomy. The scan parameters were set as follows: Field intensity

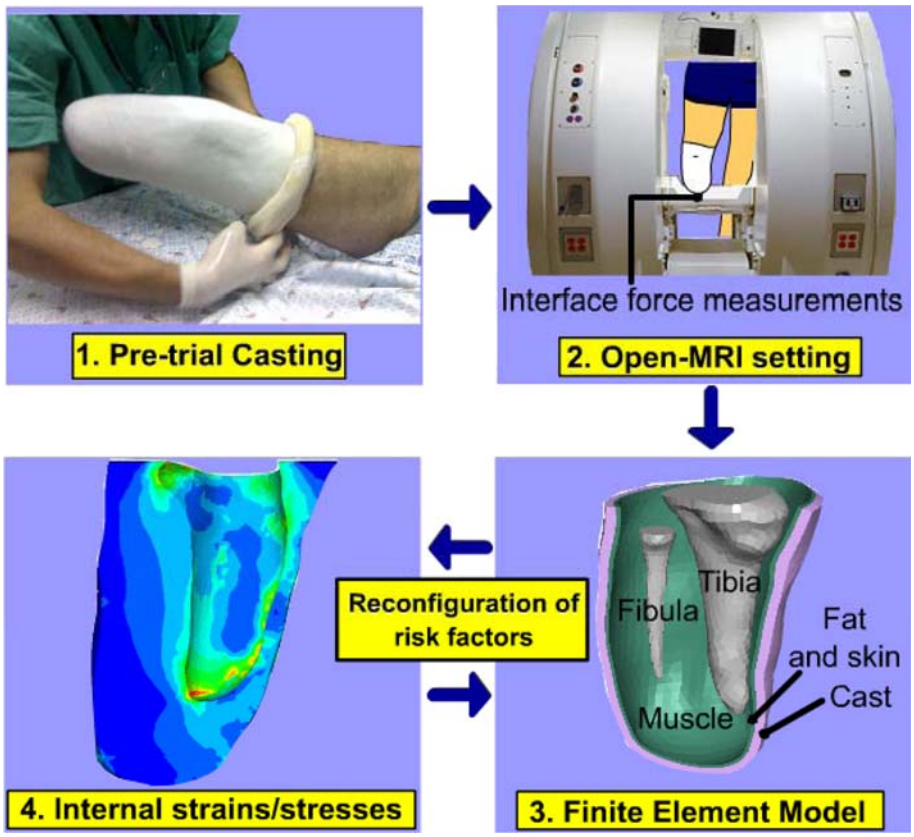

FIGURE 1. The process of patient-specific three-dimensional modeling is initiated by (1) pre-trial plaster cast preparation of the transtibial amputation residuum. The cast is used as a container for the residual limb while (2) internal anatomy images of the loaded and unloaded limb are acquired in an open-MRI. The images are used to build a (3) solid model of the residuum which is then (4) analyzed for internal strains/stresses in a finite element solver. Biomechanical risk factors for deep tissue injury or pressure ulcers are reconfigured next for further strain/stress analyses in variant model cases.

was 0.5 T, spatial resolution was 0.1 mm, and slice thickness was 4 mm. This open-MRI system was originally designed for imaging minimally invasive surgical procedures. For research applications, however, the vertical gap configuration (Fig. 1, frame #2) allows imaging in several erect patient positions. In this study, we employed the vertical gap configuration to image the internal anatomy of the residuum while the TTA patient stood inside the gap between the magnets of the MRI system, at weight-bearing and non-weight-bearing positions (Fig. 1, frame #2).

Specifically, a plaster cast replica of the residuum was created pre-trial (Fig. 1, frame #1). The cast was employed as a container of the residuum during the trial, since the patients' own prosthetic socket could not be deprived of its metallic components for the MRI scanning without damaging it for further use. We obtained axial and coronal MRI sequences of the unloaded residual limb inside the plaster cast, at a one-legged standing position. Then, the patient was instructed to apply mild loading to the residuum using his body weight against a rigid support (Fig. 1, frame #2) while a second set of scans was obtained. Contact pressures between the cast and the support were measured during this standing-like posture, using piezoresistive ultra-thin (thickness of 0.2 mm) force sensors (accuracy ±5%, capacity 440 N, FlexiForce, Tekscan Co., Boston, MA, USA) to verify weight-bearing. To exclude postural sways, we considered the maximal pressure values measured during the 5 min of the weight-bearing MRI trial. This procedure is described in more detail in Portnoy *et al.*[34]

Biomechanical Computer Modeling of the Residuum

The MRI scans of the unloaded residuum were imported into a solid modeling software (SolidWorks 2009, SolidWorks, Concord, MA, USA). A 3D solid model was created (Fig. 1, frame #3) by loading the transversal MRI scans of the unloaded residuum into parallel planes and manually differentiating between the fibula, tibia, muscle, fat, and the plaster cast per each slice. The solid model was then imported to an FE modeling software (ABAQUS v. 6.8, SIMULIA, Providence, RI, USA) for nonlinear large deformation strain/stress analyses. A skin layer with thickness of 2 mm[18] was then configured in the FE model on the outer surface of the fat tissue. The main geometrical characteristics of the TTA residuum, as reconstructed from the MRI scan of the patient, are detailed in Table 1. We will refer to this anatomy herein as being the reference case. It should be clarified that the reference anatomy in Table 1 is defined as such only for the purpose of comparing internal mechanical conditions in the residuum following modifications of the original (reference) anatomy. By no means do we suggest that the residuum described in Table 1 is in some way representative of TTA residual limbs, which, as mentioned in the "Introduction", are highly variable.

TABLE 1. Geometrical characteristics of the transtibial residuum scanned by magnetic resonance imaging as a reference anatomy for this study.

Geometrical property	Value
Length (cm)	
Tibia	11.2
Fibula	8.9
Muscle flap under the tibia	2.1
Circumference of the residuum (cm)	
At the tibial tuberosity	31
Central residuum	28
Bevelment (°)	
Tibia	52.3
Cross-sectional area (cm^2)	
At the tibial tuberosity	14.9
Central tibia	8.1
Distal tibia	1.5
Central fibula	0.6
Distal fibula	0.2
Central muscle	58.8
Distal muscle	33.6
Volume (cm^3)	
Tibia	150.8
Fibula	8
Muscle	702
Fat	90.2
Skin	92.4
Bone proximity layer (BPL)	22.2
Fat proximity layer (FPL)	14.8

Vertical motion of the shinbones relative to the plaster cast during weight-bearing was measured on the MRI coronal scans of the participating subject, by comparing the distance between the edges of the bones and the skin at the most distal point of the limb at the scans with and without load-bearing, as described in our previous paper.[34] This vertical downward motion of the bones, found to be 1.6 mm for the present subject, was then used as displacement boundary condition applied vertically to create a rigid body motion of the bones in the FE analyses to simulate load-bearing. The external cast surface was constrained for all translations. We modeled the cast as a homogeneous, isotropic, and linear-elastic material, with elastic modulus of 1 GPa and Poisson's ratio of 0.3.[3] A friction coefficient of 0.7[39] was set between the skin and the cast. "No slip" conditions were set at the bone–muscle and muscle–fat interfaces. These conditions were imposed using the "surface-to-surface" tie option in ABAQUS where the bone was the "master" surface in the bone–muscle interface, and the muscle was the "master" surface in the muscle–fat interface.

Rotational degrees of freedom were tied where applicable. The bones were assumed to be rigid. All soft tissues were assumed to be hyperelastic, homogeneous, and isotropic, and were modeled using the Generalized Mooney-Rivlin Solid strain energy function[24]:

$$W = C_{10}(I_1 - 3) + C_{11}(I_1 - 3)(I_2 - 3) + \frac{1}{D_1}(J - 1)^2 \quad (1)$$

where the invariants of the principal stretch ratios λ_i are $I_1 = \lambda_1^2 + \lambda_2^2 + \lambda_3^2$ and $I_2 = \lambda_1^{-2} + \lambda_2^{-2} + \lambda_3^{-2}$, the relative volume change is $J = \lambda_1\lambda_2\lambda_3$, and C_{10}, C_{11}, D_1 are the constitutive parameters. Values for the constitutive parameters C_{10}, C_{11}, D_1 were adopted from the literature for all soft tissues, and are specified in Table 2. The magnitudes and distributions of Green–Lagrange strains (true strains) in the soft tissues of the residuum were calculated in ABAQUS from the bone displacement boundary conditions. The second Piola Kirchoff stresses were then derived from the Green–Lagrange strains, and finally, Cauchy stresses were calculated from the second Piola Kirchoff stresses, as detailed in Portnoy *et al.*[34]

Variations Applied to the Residuum Model

Next, we studied how each of the five biomechanical factors listed in the "Introduction", that is, bone lengths, tibial bevelment, existence of a fibular osteophyte, stiffness of the muscle flap, and location of a surgical scar, potentially affect internal tissue loads. Each of these five factors was studied separately, and so, altogether, a set of model variants was created to simulate alternate hypothetical surgical outcomes of the residuum, as well as physiological or pathophysiological changes in the stiffness of the muscle flap.

In total, 12 variant model configurations were built and analyzed, as summarized in Table 3. The geometrical manipulations, i.e., shorter tibial lengths, different tibial end bevelments, and an osteophyte at the distal fibular end (Table 3), were conducted on the solid model, as described in sections "Bone Lengths", "Tibial Bevelment", and Fibular Osteophyte", respectively. Analyses where mechanical properties of the soft tissues of the TTA residuum were modified, i.e., those that tested the effect of changes in stiffness of the muscle flap tissue, and those that included scarring in different locations and depths (Table 3), were conducted by modifying the mechanical properties of elements directly in the FE model, in the ABAQUS software environment, as described in sections "Stiffness of the Muscle Flap" and "Surgical Scars".

Bone Lengths

The tibial and fibular lengths of the TTA patient, as measured directly from the MRI scans of his residuum, were 11.2 and 8.9 cm, respectively. To virtually shorten the bones, so as to simulate a higher level of TTA, we omitted equal number of transversal contours from the distal end of each bone, resulting in tibia lengths of 10.5 and 9.2 cm and corresponding fibula lengths of 8.5 and 7.4 cm. These shortened lengths are realistic, and were documented in real TTA cases studied in our previous work.[33] We recreated a dome of up to 4 mm in height on the most distal bone contour for the artificially shortened bones to virtually mimic the outcome of rounding sharp bone edges with surgical tools. The space created in the model as a result of shortening the bones was filled with muscle flap tissue, resulting in thicker muscle flaps in model configurations where bones were shortened (Fig. 2a and Table 3). Specifically, the models with shortened bones had muscle flaps that were 0.14% or 0.58% larger in volume, for the less proximal and more proximal truncations, respectively, compared to the real muscle flap volume demonstrated in the MRI scan (Table 1).

Tibial Bevelment

We chose a sagittal slice in the solid model through the tibia, at its thickest sagittal cross-section, to measure the distal tibial bevelment (Fig. 2b). A longitudinal tibial axis was first set, and the perpendicular axis with respect to this longitudinal axis was determined (Fig. 2b). The angle between the latter axis and a line which is tangent to the tibial profile gradient was considered as the distal tibial bevelment (Fig. 2b). By

TABLE 2. Constitutive parameters for soft tissues of the transtibial residuum represented using Eq. (1).

Soft tissue	C_{10} (kPa)	C_{11} (kPa)	D_1 (MPa^{-1})	Species	References
Fat	0.143	0	70.2	Ovine	[10]
Soft flaccid muscle	2.3	0	4.36	Porcine	[27]
Average flaccid muscle	4.25	0	2.36	Porcine	[27]
Stiff flaccid muscle	6.2	0	1.62	Porcine	[27]
Contracted muscle	8.075	0	1.243	Human	[14]
Skin	9.4	82	0	Human	[12]
Scar	148.9	0	0	Human	[7]

TABLE 3. Design of the model simulations and summary of outcome measures.

Variant model configurations and values for input parameters		Values of outcome measures: Mean principal compressive strain (%)		Mean principal tensile strain (%)		Mean maximal shear strain (%)		Mean strain energy density (kJ/m^3)	
Parameter type	Variation	BPL	FPL	BPL	FPL	BPL	FPL	BPL	FPL
Reference residuum model[a]		3.1 (1.3)	2.5 (1.1)	2.8 (1.4)	2.0 (0.7)	2.9 (1.3)	2.5 (0.8)	47.4 (43.4)	14.8 (12.2)
Tibial length	9.2 cm	4.5 (2.1)	1.8 (1.0)	4.2 (2.0)	1.5 (0.7)	4.6 (2.2)	1.9 (0.8)	48.2 (45.3)	10.9 (10.0)
	10.5 cm	4.6 (2.0)	2.1 (1.1)	4.3 (2.0)	1.7 (0.8)	4.7 (2.2)	2.2 (0.9)	49.8 (48.7)	13.9 (13.1)
Tibial bevelment	37.7°	4.6 (2.2)	2.4 (1.5)	4.4 (2.1)	2.0 (1.0)	4.7 (2.3)	2.5 (1.3)	51.3 (53.7)	16.6 (20.2)
	42.9°	4.9 (2.2)	2.5 (1.2)	4.7 (2.2)	1.8 (0.8)	5.0 (2.3)	2.4 (1.0)	58.0 (53.8)	17.0 (14.1)
Osteophyte	At the fibular end	4.6 (2.2)	2.2 (0.7)	4.4 (2.2)	1.6 (0.5)	4.6 (2.2)	1.9 (0.8)	50.4 (58.2)	11.5 (4.9)
Mechanical properties of the muscle flap	Soft flaccid muscle	5.9 (2.4)	3.1 (1.5)	5.5 (2.3)	2.3 (1.0)	5.8 (2.4)	3.0 (1.3)	40.5 (32.7)	15.8 (12.4)
	Stiff flaccid muscle	4.0 (1.9)	1.9 (1.0)	3.7 (1.9)	1.6 (0.7)	3.9 (1.9)	2.1 (0.9)	51.0 (51.6)	18.1 (14.3)
	Contracted muscle	3.5 (1.8)	1.6 (0.9)	3.3 (1.8)	1.3 (0.5)	3.5 (1.8)	1.6 (0.7)	53.1 (58.1)	14.7 (13.1)
Scarring	Skin-deep anterior scar	3.8 (1.9)	1.9 (1.0)	3.6 (1.8)	1.8 (0.7)	3.8 (1.8)	2.2 (0.8)	32.4 (30.2)	11.8 (9.6)
	Skin-deep inferior scar	3.8 (1.9)	1.8 (1.0)	3.6 (1.8)	1.8 (0.7)	3.8 (1.8)	1.5 (0.8)	32.3 (30.1)	10.8 (9.5)
	Fat-deep inferior scar	3.8 (1.9)	2.0 (1.0)	3.6 (1.7)	1.9 (0.6)	3.8 (1.8)	2.2 (0.8)	32.3 (29.8)	11.9 (8.9)

Variant model configurations and values for input parameters		Values of outcome measures: Mean principal compressive stress (kPa)		Mean principal tensile stress (kPa)		Mean maximal shear stress (kPa)		Mean von Mises stress (kPa)	
Parameter type	Variation	BPL	FPL	BPL	FPL	BPL	FPL	BPL	FPL
Reference residuum model[a]		3.2 (6.4)	3.8 (1.9)	1.3 (6.4)	1.5 (1.9)	0.5 (0.2)	0.4 (0.1)	0.9 (0.4)	0.7 (0.3)
Tibial length	9.2 cm	2.5 (1.1)	2.5 (0.5)	1.0 (1.2)	0.2 (0.4)	0.8 (0.4)	2.1 (0.1)	1.3 (0.6)	0.5 (0.2)
	10.5 cm	2.5 (1.2)	2.8 (0.6)	1.0 (1.2)	1.5 (0.5)	0.8 (0.4)	2.3 (0.2)	1.3 (0.6)	0.6 (0.3)
Tibial bevelment	37.7°	2.4 (1.4)	2.9 (0.8)	0.9 (1.3)	0.3 (0.5)	0.8 (0.4)	2.8 (0.2)	1.3 (0.6)	0.7 (0.4)
	42.9°	2.8 (1.4)	3.1 (0.6)	1.1 (1.4)	1.1 (0.4)	0.9 (0.4)	1.6 (0.2)	1.4 (0.6)	0.7 (0.3)
Osteophyte	At the fibular end	2.5 (1.1)	2.9 (0.5)	1.0 (1.2)	2.3 (0.5)	0.8 (0.3)	0.3 (0.1)	1.3 (0.7)	0.6 (0.2)
Mechanical properties of the muscle flap	Soft flaccid muscle	1.9 (1.0)	2.3 (0.6)	0.9 (1.0)	0.8 (0.4)	0.5 (0.2)	2.9 (0.1)	0.9 (0.4)	0.5 (0.2)
	Stiff flaccid muscle	3.1 (1.5)	3.8 (0.8)	1.2 (1.6)	2.8 (0.7)	1.0 (0.5)	3.2 (0.2)	1.7 (0.8)	0.9 (0.4)
	Contracted muscle	3.5 (1.8)	4.1 (0.7)	1.3 (1.8)	2.2 (0.5)	1.1 (0.6)	1.4 (0.2)	1.9 (1.0)	0.9 (0.4)
Scarring	Skin-deep anterior scar	1.9 (1.2)	1.8 (1.0)	0.7 (1.2)	1.6 (0.8)	1.0 (0.3)	3.1 (0.1)	1.1 (0.5)	0.6 (0.2)
	Skin-deep inferior scar	1.9 (1.2)	1.7 (1.1)	0.7 (1.2)	1.5 (0.9)	0.6 (0.3)	2.9 (0.1)	1.1 (0.5)	0.6 (0.3)
	Fat-deep inferior scar	1.9 (1.2)	1.7 (1.0)	0.7 (1.2)	1.4 (0.9)	0.6 (0.3)	2.8 (0.1)	1.1 (0.5)	0.6 (0.2)

The data are averaged in the bone proximity layer (BPL) and fat proximity layer (FPL), as depicted in Fig. 4. Values in parentheses are standard deviations from the mean. The values of the outcome measures provided for the reference residuum model were obtained in a model configuration that represents the actual geometry of the transtibial amputation patient, as measured from his MRI scan (tibial length = 11.2 cm, tibial bevelment = 52.3°, and no osteophyte or scar tissue). The constitutive properties for the muscle flap in the reference case are of "average flaccid muscle" (muscle property values are provided explicitly in Table 1). No scar was included in the reference case.
[a]A detailed specification of the reference anatomy is provided in Table 1.

expanding the anterior aspect of distally located contours of the tibia, according to the shape of proximal contours, we were able to produce "additional bone" in the models, functioning as milder tibial bevelments (Fig. 2b). Thus, we reduced the actual tibial bevelment of 52.3° measured from the original MRI scans to 42.9° and then to 37.7° (Fig. 2b), again, as to simulate a "what if" scenario where the orthopedic surgeon conducting the amputation would produce a milder bevelment. These bevelments are realistic, and occur in some TTA.[43] Also, the milder tibial bevelments, which artificially added bone tissue component to the model, consequently reduced the muscle flap volume (Table 1), by approximately 0.05%.

Fibular Osteophyte

To simulate an osteophyte developing at the distal end of the original fibula of the TTA patient (that had no osteophyte), we added transversal contours with decreasing circumferences to create a typical cone-shaped ossification as depicted in Fig. 2c. To allow

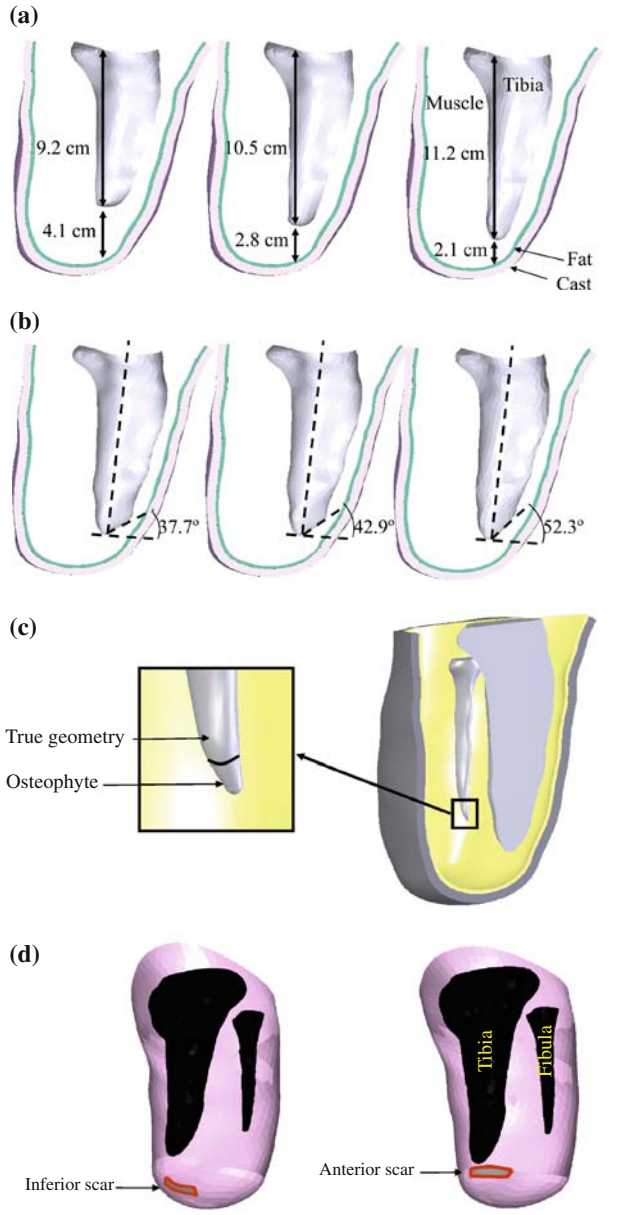

FIGURE 2. The residuum models for (a) tibial lengths of 9.2, 10.5, and 11.2 cm; (b) distal tibial bevelments of 37.7, 42.9, and 52.3°; (c) a fibular osteophyte; and (d) scar locations and depths seen from a lateral-oblique view.

space for the addition of an osteophyte, the volume of the muscle flap component of the model (Table 1) was reduced by 0.12%.

Stiffness of the Muscle Flap

Different stiffnesses of the muscle flap were applied to the entire muscular bulk to simulate the biomechanical consequences of either voluntary contraction of the flap, or spasm resulting in knee flexion contracture,[46] or different levels of flap flaccidity (Tables 2 and 3). Specifically, in prior experiments, we found that the shear modulus of a flaccid muscle deformed perpendicularly to its fibers is 8.5 ± 3.9 kPa (mean ± standard deviation, SD).[27] Consistent with these findings, we conducted three separate analyses where we applied the mean value, the mean + 1 SD and the mean – 1 SD to simulate biological variability of muscle stiffnesses across patients with a flaccid muscle flap (constitutive properties are specified in Table 2). Additionally, we considered a 90% stiffening of the muscle flap to simulate voluntary or spastic contraction (Table 2) based on the data of Hoyt *et al.*[14] As the TTA patient in this study was instructed to relax the muscles of his residuum during the scans, we will refer to the analysis conducted with the mean shear modulus attributed to flaccid muscle as the reference case (Tables 2 and 3).

Surgical Scars

Inclusion of surgical scars in FE models of a TTA residuum is likely to be important for realistically simulating the internal mechanical interactions in and between the soft tissues, and this has been done here for the first time in the literature (Tables 2 and 3). We referred to the nonscarred residuum model as the reference case (Table 3). We selected several adjacent elements from the skin mesh in the FE model where a surgical scar can be expected, according to clinical experience of the senior surgeon (ISN) and the post-amputation rehabilitation physical therapists (ZY, AK) co-authoring this article. We then assigned these elements mechanical properties of scar tissue (Table 2). We ran two analyses in which superficial scars, with length of ~2.5 cm, width of ~0.6 cm, and thickness of ~2 mm, were placed at the inferior or anterior aspect of the residuum (Fig. 2d and Table 3). In a third scarring analysis, we deepened the inferior scar to the fat tissue, creating a scar that is clinically termed adherent scar, with thickness of 4.6 mm. The volume of each scar in the scarring models is given in Table 4.

The Numerical Method

The mesh of the FE model is depicted in Fig. 3, where mesh examples of different tibial lengths, bevelments, fibular osteophyte, and scarring are shown. We used the "free meshing" option in ABAQUS for all model components. We verified that all meshes consisted of elements that hold an aspect ratio smaller than 10 between the longest and shortest element edge. The bones were meshed with 1460 to 1563 4-node quadrilateral surface elements ("SFM3D4" in

TABLE 4. The volumes, mean strains, mean strain energy density, and mean stresses of the scar tissues in the scarred models (Fig. 2d and Table 3).

Scar location and depth	Volume (mm^3)	Mean principal compressive strain (%)	Mean principal tensile strain (%)	Mean maximal shear strain (%)	Mean strain energy density (kJ/m^3)	Mean principal compressive stress (kPa)	Mean principal tensile stress (kPa)	Mean maximal shear stress (kPa)	Mean von Mises stress (kPa)
Skin-deep anterior scar	300	0.2 (0.2)	0.7 (0.3)	0.4 (0.2)	27.5 (16.8)	0.1 (0.4)	7.3 (2.4)	3.7 (1.1)	6.7 (2.1)
Skin-deep inferior scar	300	0	0.4 (0.1)	0.2	11.9 (4.3)	0	5.1 (1.0)	2.6 (0.5)	4.6 (0.8)
Fat-deep inferior scar	690	0.3 (0.3)	0.3 (0.2)	0.3 (0.2)	10.9 (14.6)	1.6 (0.9)	2.6 (2.6)	2.1 (1.2)	3.7 (2.1)

Values in parentheses are standard deviations from the mean.

ABAQUS; number of bone elements depended on the bone lengths in the specific model configuration, as in Figs. 2a and 3 and Table 3). The bone mesh density was such that the inter-nodal spacing at the distal tibial end was approximately 2 mm (Fig. 3) which appeared, in preliminary analyses, to be sufficient in minimizing edge effects at the bone proximity. The muscle flap was meshed with 33757 to 34523 second-order 10-node modified quadratic tetrahedron elements (''C3D10M''), and again, the specific number of elements depended on the volume of the muscle flap as detailed above. The fat tissue was meshed with 6011 to 7831 10-node tetrahedron elements (''C3D10M''). The same element type was used for the 23 elements of the adherent (deep) scar that was assumed to be contained in the fat component in one analysis (Table 3). The skin tissue was meshed with 2098 to 2659 6-node quadratic triangular membrane elements (''M3D6''). When skin-deep (i.e., superficial) scar tissue was incorporated in the models (Table 3), these scars were meshed with 6 to 11 3-node quadratic triangular membrane elements (''M3D3''). The cast was meshed with 1962 to 2110 (''C3D10M'') elements. Our nonlinear models were solved iteratively in ABAQUS using the Newton–Raphson method. The convergence criteria that were used throughout the ABAQUS analyses were set as $R_\alpha^n = 0.005$ for residual forces or moments and as $C_\alpha^n = 0.01$ for displacement corrections. The mesh density was refined in preliminary simulations, where it was found that denser meshes than the ones reported above substantially increased the runtime but had negligible effect (of $<5\%$) on the strain/stress results. The runtime of a strain/stress analysis of each given model configuration was approximately 10 h using 64-bit Pentium-class workstation equipped with 4 GB RAM and with a designated graphic processor board recommended for use with ABAQUS. Some of the analyses with the denser meshes (e.g., the one with the osteophyte) were conducted on a Linux-based 2 CPU ALTIX XE Silicone Graphics computer (Silicone Graphics Inc., Sunnyvale, CA, USA) having a total of 8 cores and 16 GB of memory. This reduced the runtime to approximately 4 h. The sizes of the model files (.cae suffix in ABAQUS) ranged from 10 to 23 MB per each model variant, and the sizes of the results files (.odb suffix in ABAQUS) ranged from 105 to 380 MB per each model variant.

Outcome Measures and Data Analysis

We calculated distributions of principal compression strain/stress, principal tension strain/stress, maximal shear strain/stress, strain energy densities (SED), and von Mises stresses. Strains are reported here as

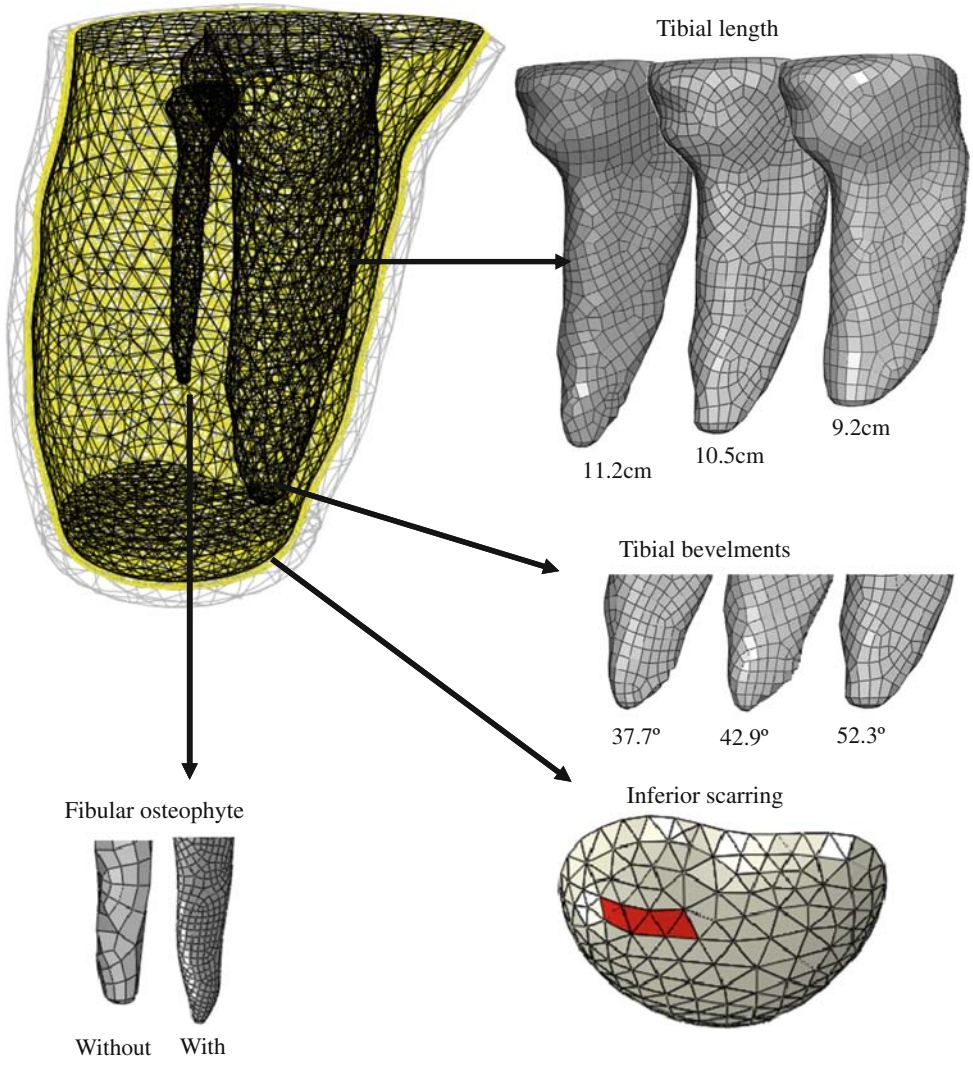

FIGURE 3. The mesh of the finite element model of the transtibial amputation residuum that consists of the tibia, fibula, muscle, fat, skin, and the enveloping plaster cast. The geometric manipulations, i.e., tibial length, tibial bevelment, fibular osteophyte, and scarring, are also depicted.

engineering strains, and stresses are reported as Cauchy stresses.

We defined a reference residuum model (Table 3)—as a model representing the actual geometry of the TTA patient, measured from his MRI scan (Table 1). The constitutive properties for the muscle flap in this reference case are of "average flaccid muscle" (property values are provided explicitly in Table 2). No scar was included in the reference model to isolate the effects of scars on predicted strain/stress measures by comparing the scarring configurations to the reference case.

For the purpose of comparing internal tissue loads across variant model configurations (Table 3), and primarily, for identifying which of the surgical/physiological factors more dominantly affected the deep layer of the muscle flap (as opposed to more superficial tissues), and thus can be associated with DTI, we defined two separate volumes of interests (VOI) containing muscle tissue elements. The first VOI is a layer consisted of all the muscle flap elements contacting the third distal end of the tibia, as shown in Fig. 4. We will refer to this VOI herein as the bone proximity layer (BPL) of muscle flap tissue (Fig. 4). The second VOI consisted of all the muscle flap elements contacting the fat tissue, that are under the projection of the distal third of the tibia, and that are located not higher than the height of the distal third of the tibia, again as shown in Fig. 4. We will refer to this second VOI as the fat proximity layer (FPL) of the muscle flap (Fig. 4). The number of elements in the BPL and FPL slightly changes between model variants, but was approximately a minimum of 350

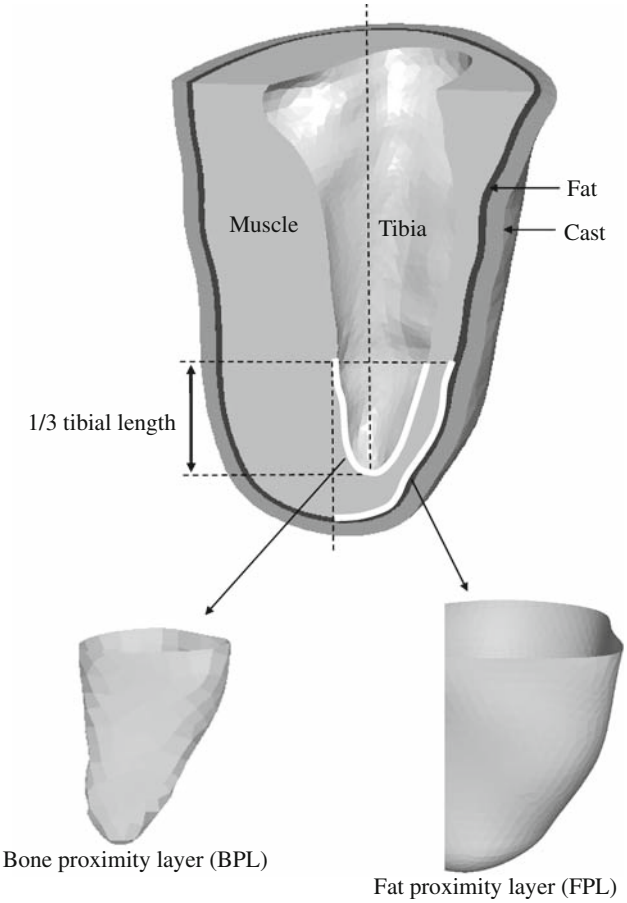

FIGURE 4. Definition of the volumes of interest (VOI) for strain/stress analyses and comparisons across variant model configurations. We defined two VOI consisting of muscle flap elements in the finite element solver: the first VOI consisted of all the muscle elements touching the third distal end of the tibia (marked as the bone proximity layer—BPL). The second VOI consisted of all the muscle flap elements contacting the fat tissue, that are under the projection of the distal third of the tibia, and that are located not higher than the height of the distal third of the tibia (marked as the fat proximity layer—FPL).

elements for the BPL and 450 elements for the FPL. The thicknesses of both the BPL and FPL were about 6 mm.

For each model configuration, we averaged strains, SED, and stresses across elements separately for each VOI (Table 3). As a second measure of muscle tissue exposure to high sustained loads, we also calculated the volumes (in mm^3) of BPL and FPL that hold von Mises stresses above 2 kPa, and then normalized these volumes by the total volumes of the BPL and FPL in each variant model configuration, respectively (Table 1). This 2 kPa threshold was selected because our previous studies in rat models of DTI showed that muscle tissue remains viable for at least 4 h if stresses below 2 kPa are applied.[21]

RESULTS

The mean of these maximal contact pressure recordings was 24 kPa (averaged over the cast-table contact area) with a SD of ±3 kPa. The corresponding mean contact pressure calculated at the inferior surface of the cast, in the reference FE model, was 25 kPa, which is in good agreement with the above measurements. The values of strains, SED, and stresses, averaged across the BPL and FPL, are presented in Table 3 for each of the 12 variant model configurations. The percentage volumes of muscle tissue at the BPL and FPL that hold von Mises stresses above 2 kPa are presented in Fig. 5 for all the model variants.

Generally, strains, SED, and stresses at the BPL were higher than the corresponding values at the FPL, e.g., as in the reference case where mean strains were approximately 27% higher in the BPL than in the FPL (Table 3). The mean SED at the BPL in the reference case was approximately threefold higher than in the FPL which indicates that muscle tissue deformations intensify adjacent to the truncated tibia. Sliding of the skin against the socket occurred in all analyses, and was found to be 0.7 ± 0.56 mm (mean ± SD). The maximal sliding occurred under the tibia and along the tibial shaft. The model variant which showed the maximal skin sliding was the adherent inferior scar model, for which the peak sliding was 1.6 mm.

Bone Lengths

The von Mises stress distribution in muscle flap tissue at the bone ends (depicted in Fig. 6 using transversal views directly under the bones) shows a larger region subjected to elevated von Mises stresses in the muscle tissue underlying longer truncated bones. This occurred both under the tibia and fibula (Fig. 6). Analysis in a sagittal cross-section shows that the longer bone configurations also spread the loads toward the FPL (Fig. 7). Specifically, increasing the tibial length from 9.2 to 10.5 cm and then to 11.2 cm caused an increase of ~20 and ~40% in the mean strains (compression, tension, and shear) in the FPL, respectively (Table 3). Likewise, increasing the tibial length leads to increases in SED (by 36% for a 11.2-cm-long tibia; Table 3), and in principal compression stresses in the FPL (by 12% for a 10.5-cm-long tibia, and by 52% for a 11.2-cm-long tibia; Table 3).

Though the shorter tibia configurations concentrate most of the strains/stresses at the BPL rather than at the FPL (Table 3), these loads are still lower in value than peak loads that develop at the model variants with the longer bones (Fig. 7). Importantly, we found that when shortening the truncated bones from 11.2 to 9.2 cm, and thereby creating a thicker muscle flap

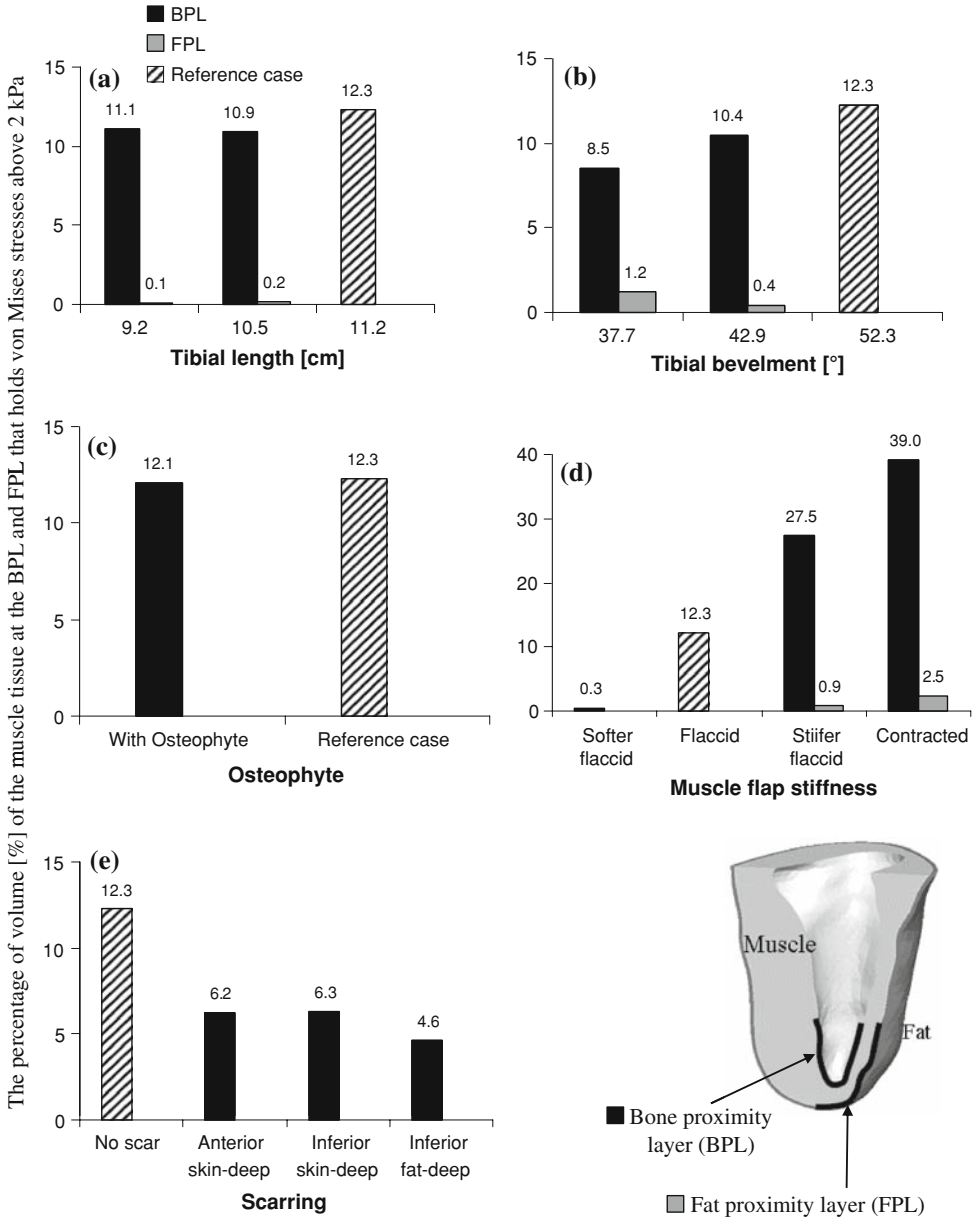

FIGURE 5. The percentage volume of muscle flap tissue in the bone proximity layer (BPL) and fat proximity layer (FPL) that hold von Mises stresses above 2 kPa for (a) different tibial lengths, (b) bevelments, (c) fibular osteophyte, (d) muscle flap stiffnesses, and (e) different scar locations and depths.

(by ~95%), peak loads at the distal edges of the bones, predominantly stresses, were relieved considerably (e.g., by up to ~80% for von Mises stresses under the tibia). The von Mises stresses at the FPL were mostly lower than 2 kPa for all the model variants of bone length (Fig. 5a).

Tibial Bevelment

The stress distributions at a sagittal cross-section for different distal tibial end bevelments are depicted in Fig. 8. Decreasing the distal tibial end bevelment from 52.3° to 42.9° and then to 37.7° consistently decreased the percentage of muscle flap volume exposed to von Mises stresses above 2 kPa in the BPL (Fig. 5b). Contrarily, this decrease in tibial bevelment caused an increase in the percentage of muscle flap volume exposed to von Mises stresses above 2 kPa in the FPL (Fig. 5). The highest bevelment (52.3°), which was the actual bevelment of the patient scanned by MRI, practically did not induce volumetric exposure to von Mises stresses above 2 kPa in the FPL (Fig. 5b).

Mean strains (compression, tension, and shear) in the BPL increased by ~70% when decreasing the tibial

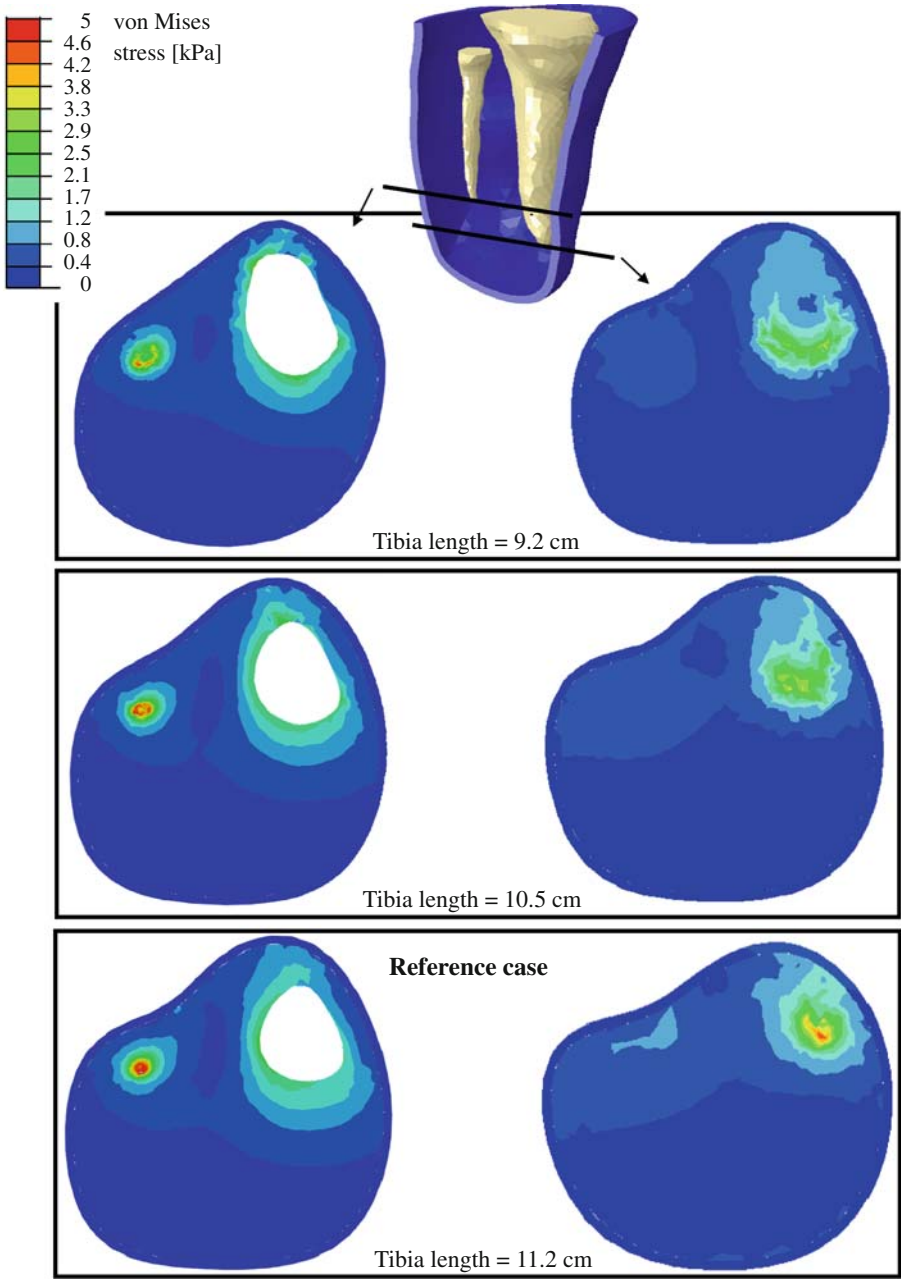

FIGURE 6. The von Mises stress distributions in muscle and fat tissues in transversal views cutting directly under the distal ends of the tibia (right frames) and the fibula (left frames) for tibial lengths of 9.2, 10.5, and 11.2 cm.

bevelment from 52.3° to 42.9°, but strains remained similar when further decreasing the bevelment to 37.7° (Table 3). The SED for the BPL showed a similar trend (Table 3). While mean principal compression and tension stresses in the BPL decreased by ~10% when decreasing the tibial bevelment from 52.3° to 42.9°, the mean shear stresses increased by ~80%, thereby causing a ~60% increase in the mean von Mises stresses in the BPL (Table 2). Decreasing the bevelment further, to 37.7°, caused an additional ~30% decrease in compression stresses in the BPL, but only slight changes in other stress components. In the FPL, mean strains and SED did not change considerably when decreasing the tibial bevelment (Table 3); however, mean principal compression and tension stresses were ~30% lower, and shear stresses escalated by more than 400% when the tibial bevelment was decreased (Table 3). We therefore find that sharper tibial bevelments increase tissue loads at the FPL (Figs. 5b and 8), particularly shear stresses (Table 3),

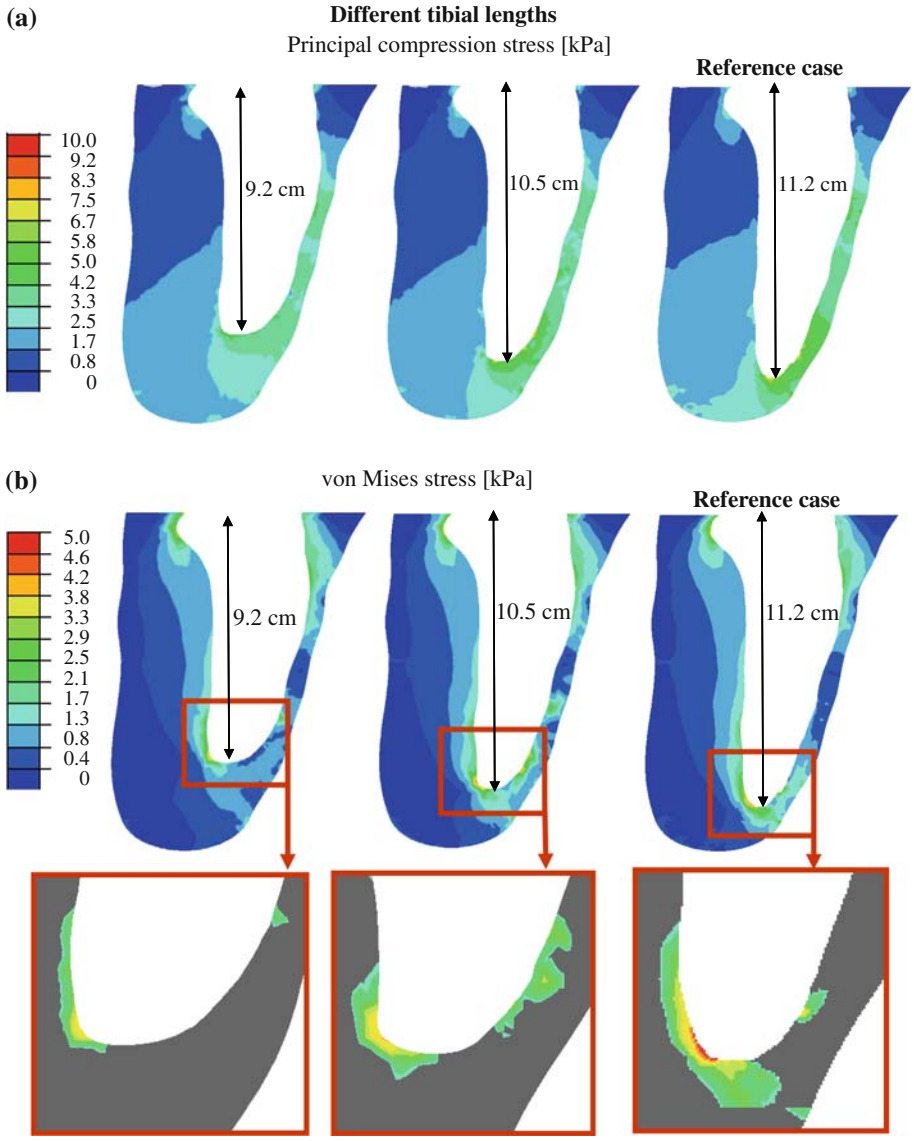

FIGURE 7. The (a) principal compression stress and (b) von Mises stress in the muscle tissue of variant model configurations with tibial lengths of 9.2, 10.5, and 11.2 cm. The distal tibial end is magnified to display "hotspots", where "safe" areas, subjected to stresses below 2 kPa, are colored gray and areas at risk, holding stresses above the 2 kPa injury threshold, are brightly colored.

but decrease tissue loads at the BPL with respect to blunt tibial edges (Fig. 5b).

Fibular Osteophyte

Generally, strains and stresses at the BPL increased mildly in the presence of the added fibular osteophyte but no trends of effects could be identified for the FPL (Fig. 9, Table 3). As could be foreseen, the fibular osteophyte concentrated stresses in muscle flap tissue around the distal tip of the fibula, but had negligible effects on tissue loads adjacent to the tibia (Fig. 9). The percentage volume of muscle flap elements subjected to von Mises stresses above 2 kPa in the BPL nearly did not change (~0.2% decrease) when the osteophyte was included (Fig. 5c). The volume of von Mises stresses above 2 kPa at the FPL was nearly zero for the model configurations with and without the osteophyte (Fig. 5c). There appeared to be a 6% increase in the mean SED in the BPL in the presence of the osteophyte; however, as calculated throughout our analyses, the SD of mean SED values was the highest (Table 3), so this change can also be considered insignificant. Overall, the fibular osteophyte caused a focal increase in mean strain and stress values in muscle flap tissue in its

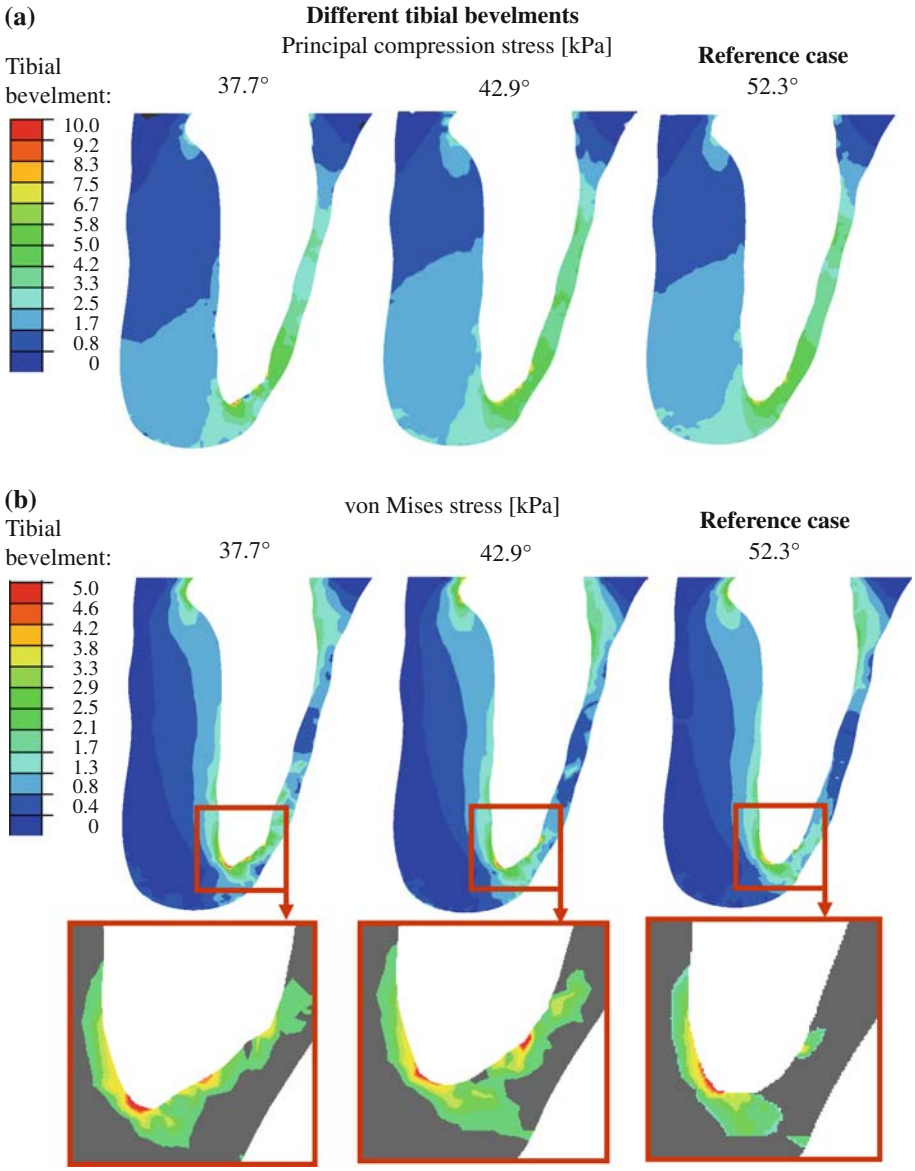

FIGURE 8. The (a) principal compression stress and (b) von Mises stress in the muscle tissue of variant model configurations with tibial bevelments of 37.7, 42.9, and 52.3°. The distal tibial end is magnified to display ''hotspots'', where ''safe'' areas, subjected to stresses below 2 kPa, are colored gray and areas at risk, holding stresses above the 2 kPa injury threshold, are brightly colored.

immediate vicinity (by ~120% for strains, ~95% for stresses), but did not induce substantial changes in strains/stresses in wider or other tissue regions (Fig. 9).

Stiffness of the Muscle Flap

Increasing the stiffness of the muscle flap tissue caused an increase in the percentage volume of muscle flap elements subjected to von Mises stresses above 2 kPa at both the BPL and FPL (Fig. 5d). However, this volumetric exposure to stresses increased more rapidly with rising muscle stiffness for the BPL than for the FPL (Fig. 5d). The increase in SED and stresses with increasing muscle stiffness is also demonstrated in a sagittal cross-section in Figs. 10b–10d. The mean von Mises stresses at the BPL were approximately twofold higher in the contracted muscle when compared to the reference case of the flaccid muscle (Table 3). The mean strains at the BPL and the FPL generally decreased when muscle stiffness was increased, as expected (Table 3). For example, in the FPL, the mean strains were 80–90% higher for the soft flaccid muscle, as compared with the contracted muscle (Tables 2 and 3). The most important finding in this

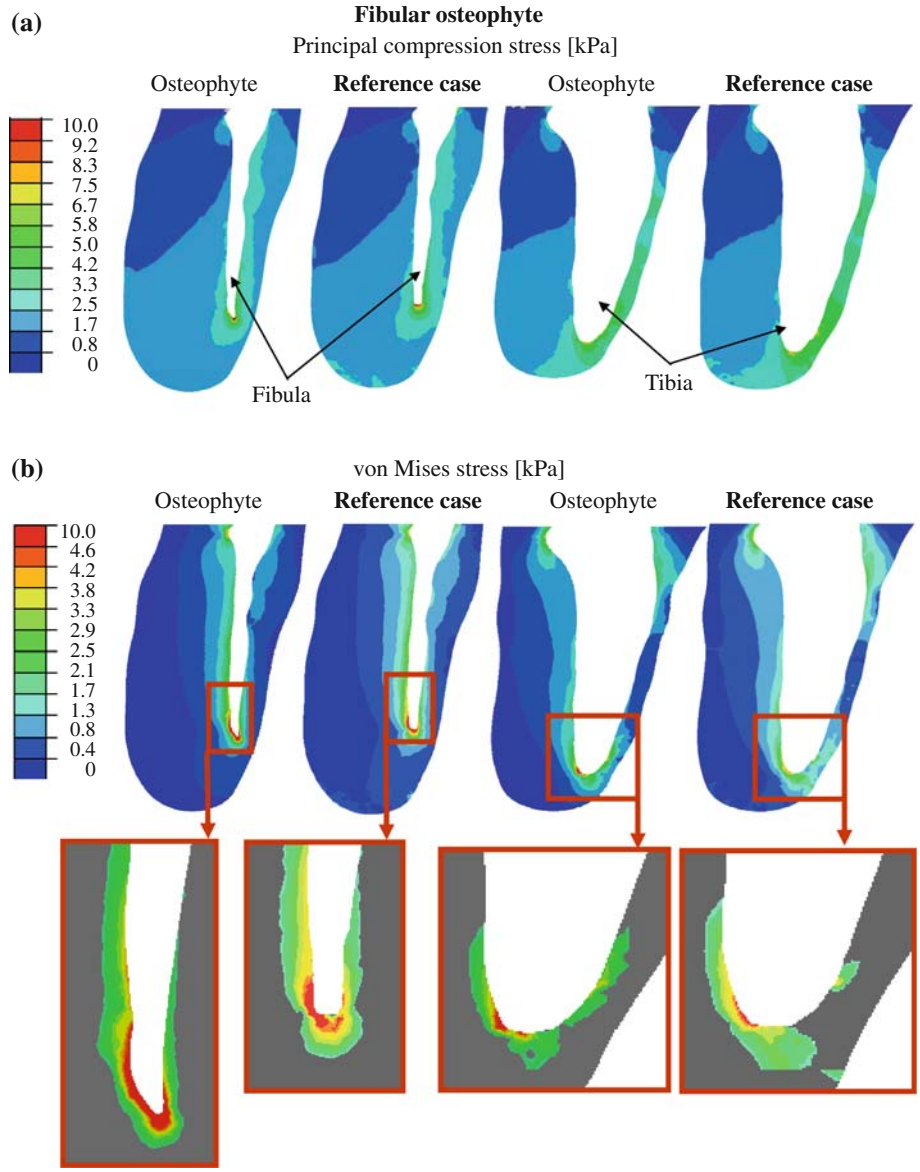

FIGURE 9. The (a) principal compression stress and (b) von Mises stress in the muscle flap tissue of the reference case model and of a variant with an osteophyte at the distal fibular end. The sagittal views are through the fibula (left two frames) and through the tibia (right two frames). The distal tibial end is magnified to display "hotspots", where "safe" areas, subjected to stresses below 2 kPa, are colored gray and areas at risk, holding stresses above the 2 kPa injury threshold, are brightly colored.

section of the analyses is that stresses at the BPL increase substantially (i.e., by up to twofold) for a contracted muscle flap or a spastic muscle flap when compared to a flaccid muscle flap.

Surgical Scars

There were only slight differences between values of mean strains, SED, and stresses in the muscle flap between variant model configurations that considered scarring, as referring to the location and depth of the scars (Table 3). The values of strains, SED, and stresses, averaged for each scar, are listed in Table 4.

When applying surgical scars to our FE model, the percentage volume of von Mises stresses above 2 kPa at the BPL decreased by at least 50% (Fig. 5c). There was no apparent difference in the percentage volume of stresses above 2 kPa when altering the scar location but for the adherent fat-deep scar the percentage volume of stresses mildly decreased (Fig. 5c). The volume of von Mises stresses above 2 kPa at the FPL was negligible in all scarring configurations (as well as in the reference case; Fig. 5c). Sagittal slices show the deviation in von Mises stresses around the distal tibial end for the different locations and depths of scars (Fig. 11). In the reference case model (i.e., with no scar tissue), stresses

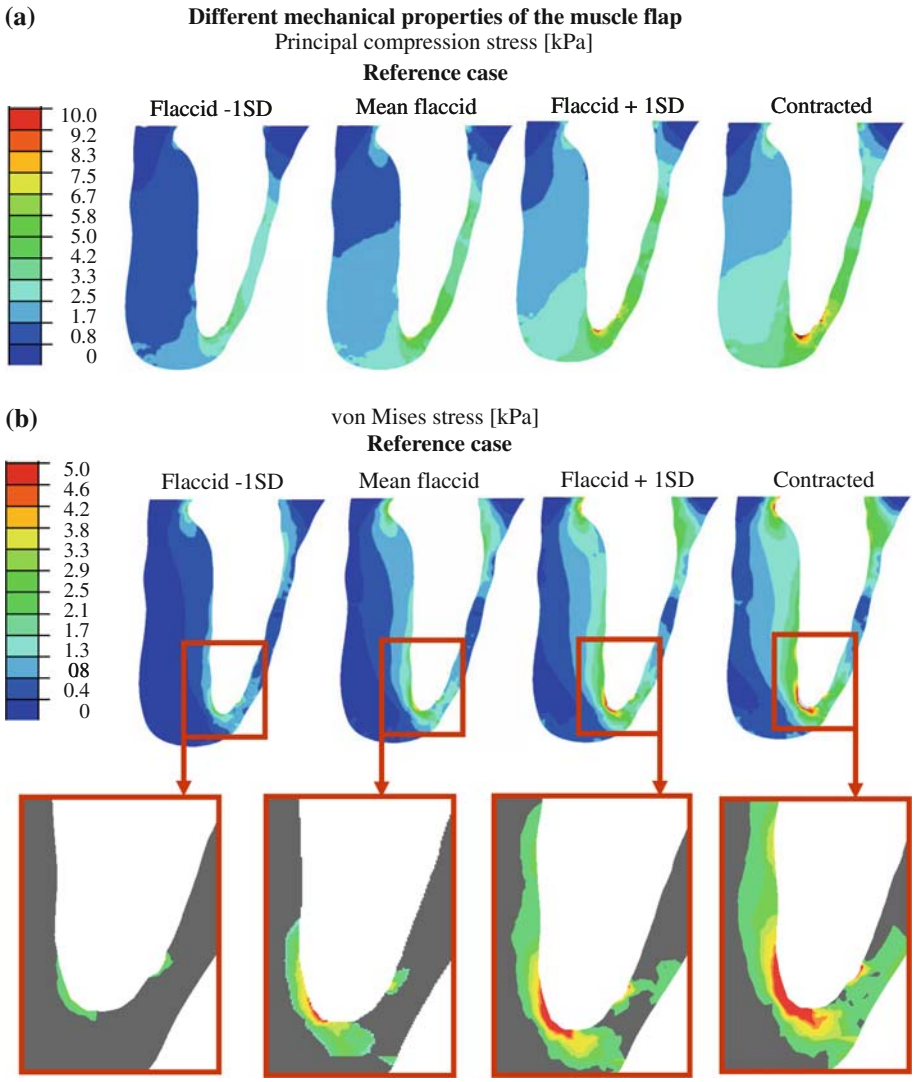

FIGURE 10. The (a) principal compression stress and (b) von Mises stress in the muscle tissue of variant model configurations with different levels of stiffness of the muscle flap (as detailed in Tables 2 and 3). The sagittal views are through the tibia. The distal tibial end is magnified to display "hotspots", where "safe" areas, subjected to stresses below 2 kPa, are colored gray and areas at risk, holding stresses above the 2 kPa injury threshold, are brightly colored.

in the muscle flap adjacent to the distal tibial end peaked at the posterior aspect of the bone (Fig. 11, upper right frame). However, after introducing scarred tissue to the skin layer, the peak stresses shifted to an inferior-anterior aspect of the bone, and this phenomenon was similar for both anterior and inferior scar locations (Fig. 11, left frames). When considering an inferior adherent fat-deep scar, stresses accumulated directly above the scar (Fig. 11, bottom right frame). The effect that scars had on the von Mises stress distribution at the skin surface is shown in Fig. 12.

Taken together, the surgical scar simulations indicated that locating a scar in different sites and depths of the residuum had the least significant effect on the overall loading of the muscle flap compared to all the other factors examined above (stresses changed by $<7\%$ across the different scars). However, with respect to the reference case that had no scar, the scar simulations were distinct in strain/stress values as well as locations of elevated strains/stresses (Table 3, Fig. 11), which strongly indicates that it is important to include surgical scars in the FE modeling for realistic representation of residual limbs.

DISCUSSION

In this study, we used computational modeling that enables isolation of the influence of individual surgical and physiological factors, i.e., the tibial length and

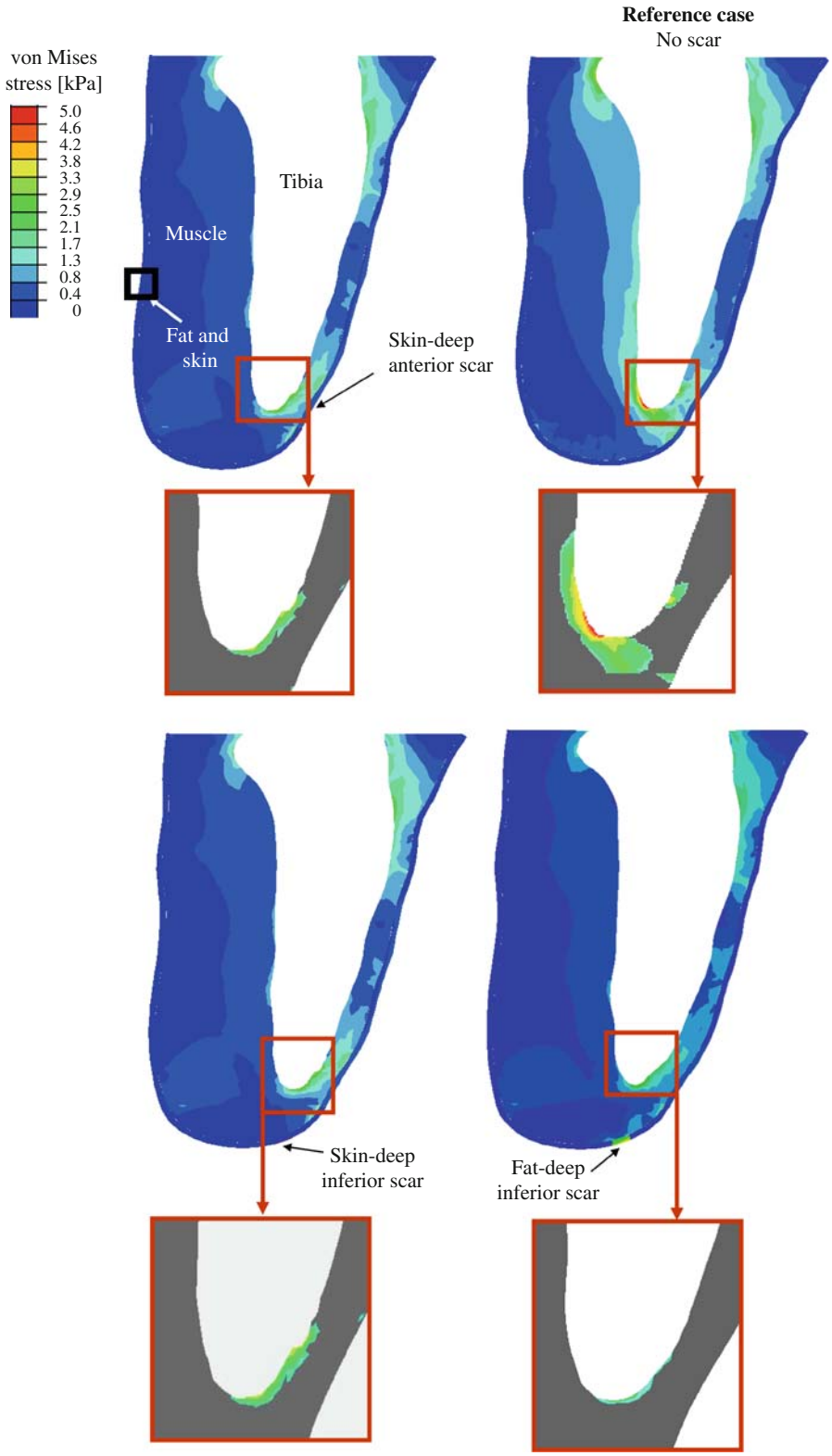

FIGURE 11. The von Mises stress distributions in the muscle, fat, and skin tissues in a sagittal view through the tibia to show the effects of scars on internal tissue stresses. The reference case of a non-scarred residuum model is depicted in the upper-right frame. The arrows on the three remaining frames point to the scar locations: skin-deep anterior scar (top left frame), skin-deep inferior scar (bottom left frame), and fat-deep inferior scar (bottom right frame). The distal tibial end is magnified to display ''hotspots'', where ''safe'' areas, subjected to stresses below 2 kPa, are colored gray and areas at risk, holding stresses above the 2 kPa injury threshold, are brightly colored.

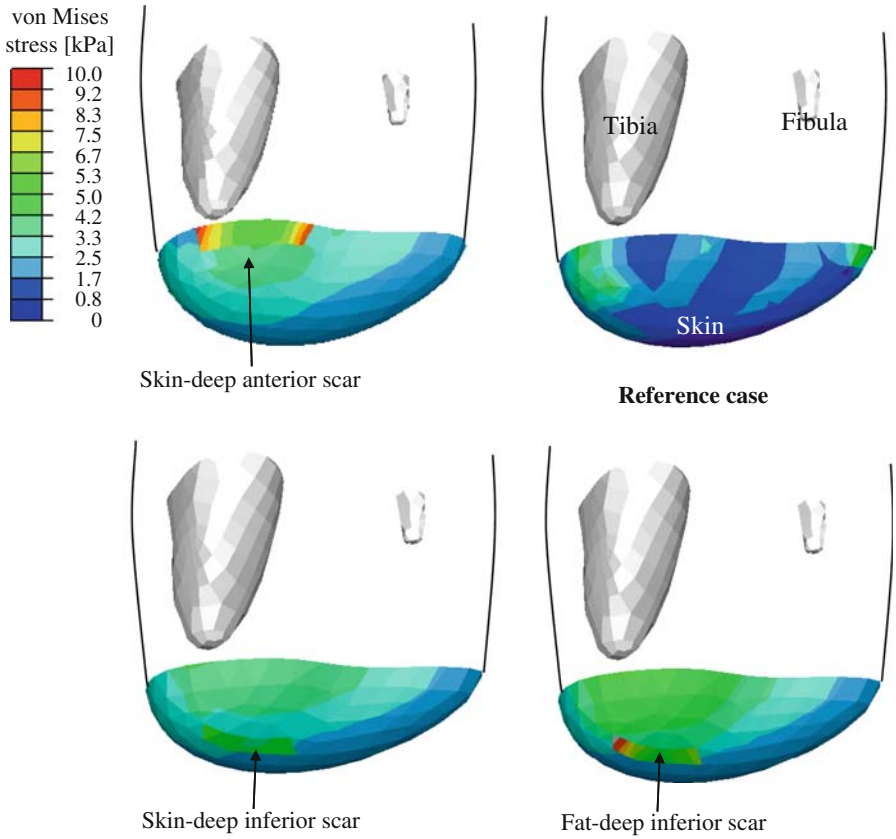

FIGURE 12. The von Mises stress distribution on the skin tissue of the non-scarred reference residuum model (upper right frame), skin-deep anterior scar (top left frame), skin-deep inferior scar (bottom left frame), and fat-deep inferior scar (bottom right frame). Proximal skin tissue has been made transparent to show the orientation of the bones.

bevelment, fibular osteophyte, muscle flap stiffness, and the location and depth of the surgical incision, on the 3D internal strain/stress distribution in the TTA residuum. Our main focus was the 3D mechanical state within the muscle flap of the TTA residuum. Since muscle tissue is more susceptible to deformation-related damage as compared to skin and fat tissues (see Agam and Gefen[1] for a review of literature on this topic), we specifically aimed at determining the mechanical conditions of muscle tissue under the distal edge of the tibia which transfers most of the body load to the muscle flap. We surmised that strain/stress concentrations in muscle flap tissue adjacent to the edges of the truncated bones is a critical catalyst in the initiation of DTI in TTA patients. As recently demonstrated by Oomens *et al.*[26] using a set of simple two-dimensional FE simulations of bone–soft tissue interactions, our results clearly show the complex, combined effects of bone geometry and mechanical properties of the contacting load-bearing soft tissues on their internal mechanical state.

Based on the contact pressure recordings that we conducted during the MRI trial (see section "Results"), and given the measured cross-sectional area of the residuum (Table 1), we evaluate that the subject applied approximately 20% of his body weight to load the cast-confined residual limb during the MRI trial. This is reasonable considering that (a) it is well known that unilateral TTA patients load their residual limb less than they load their sound limb,[25] (b) the subject did not use his own prosthesis, and (c) the MRI setting was not a natural environment for the subject. The two latter issues very likely caused the patient to feel less comfortable, and so, to load his residuum less than he would normally do in his own natural environment, and with his own prosthesis.

Consistent with our previous analysis of internal loads in the soft tissues of a residual limb of one TTA subject,[34] who was a different subject than the one whose MRI scan was used to develop the models herein, we find here higher strains and stresses developing in the bone edge proximity rather than in outlying soft tissues (Table 3, Figs. 5–11). We deliberately characterized values of each strain and stress component, and also of scalar measures of tissue loads, i.e., SED and von Mises stress, in view of an ongoing work to find injury threshold of muscle tissues that are based on either strain or stress.[9,11,21,26]

Overall, our analyses showed that shorter bones coupled with a thicker muscle flap result in lower mean strains, mean SED, and mean stresses at the FPL of the muscle flap. In the BPL, there is no such apparent trend of the mean strains and stresses; however, Fig. 6 shows a decrease in peak von Mises stresses under shorter bones. We attribute the decrease in muscle loads under shorter bones to two factors: first, the shorter bone is supported by a thicker muscular layer, dispersing the loads more uniformly and second, there is an increase in the cross-sectional area of the tibia that contacts the muscle flap for the more proximal amputation levels. Anatomically, the tibia broadens toward the knee, so that a proximal amputation level results in a larger bone–muscle contact area at the bone edge (see for example the growing widths of the distal tibial edge for shorter bones in Fig. 7). A larger bone indentation area is a factor contributing to better distribution of stresses adjacent to the contact site.[32] Since the current surgical literature recommendations are prone to a more distal amputation level,[43] as for better suspension and control of the prosthesis,[15] the truncated bones could be too sharp, which increases the risk for DTI. A proposed solution to the sharp distal edges of the truncated bones is a surgical technique, named the Ertl technique, which creates a distal tibio-fibular bone bridge that connects the tibia and fibula, and thereby increases the bone–muscle contact region.[8] The technique is claimed to enable comfortable weight-bearing at the distal end of the residual limb by creating an enhanced stable platform. It is expected that the larger surface area of the conjoint bones will dissipate the stresses more evenly. However, there is no current clinical evidence of the precedence of TTA bone-bridging over conventional surgical techniques.[29] As mentioned in the "Introduction", the commonly accepted surgical procedure in TTA is to shorten the fibula so that the distal fibular end in the residuum is approximately 2–3 cm above the distal tibial end. In our present modeling, we represented this commonly accepted surgical technique. We did not investigate the effect of shortening each bone separately, on internal loads in the residuum, since this is not a situation normally encountered in real-world scenarios (though in some special circumstances the fibula might be removed completely, or kept at the same length of the tibia for bone-bridging purposes[29]). The issue of whether to shorten the fibula more or less than what is acceptable in nowadays common practice warrants future investigation. We conclude that although mean strains and stresses at the BPL do not show a particular trend when shortening the bones, the von Mises stress at the distal edges of the bones are relieved considerably (Fig. 6), thereby theoretically decreasing the risk for DTI.

Decreasing the tibial bevelment caused propagation of internal stresses from the BPL toward the FPL VOI of the muscle flap (Fig. 5), thereby also theoretically reducing the risk for DTI. This finding may not hold for gait or other dynamic activities, because internal tissue loads there would depend not only on the extent of the bevelment, but also on the angles at which dynamic forces are transferred from the socket to the residuum.

Adding a fully-calcified osteophyte at the distal fibular end had the least influence on the overall loading of the muscle flap (Figs. 5 and 9). The osteophyte mostly increased the strain and stress concentrations locally, directly under the fibula. Specifically, the spike-like bony edge caused—as might have been expected—a concentration of high strains and stresses, which may endanger the muscle flap contained in that region. The strains and stresses under the tibia, in the BPL, increased mildly and there was no remarkable effect on the strains and stresses in the remote area of the muscle flap, at the FPL. This last finding is reasonable since the fibula and the FPL (as defined herein) are positioned in relatively distant locations within the residuum bulk (4.5–5.5 cm apart), and so, the osteophyte is located too far away to affect loads at the tibia edge region.

Elevation of muscle stiffness, simulating biological and pathobiological variation across TTA patients as well as episodes of muscle contraction or spasm, was the most influential factor to affect the rise of von Mises stresses at the FPL, and also had an effect of escalation of von Mises stresses at the BPL (Fig. 5). This last finding suggests that, theoretically, a stiffer muscle flap is more prone to developing DTI as well as superficial PU. The clinical relevance of this finding is administration of botulinum toxin type B (Botox) injections directly to spastic muscles in the residuum to prevent involuntary muscle flap contractions and related pain.[16] Based on our present findings that stiffer muscle tissue is more susceptible to DTI and PU, Botox injections might theoretically also protect from DTI and PU.

The shifting of the stress distribution near the distal end of the tibia when locating a surgical scar in different sites and/or depths of the residuum, depicted in Fig. 11, may be an important factor affecting the viability of the muscle flap. This is because vascularization is not uniform in the flap (primarily under the tibia) and so, the ideal is to shift loads to more vascularized regions which have a better chance of maintaining adequate perfusion under loading. This suggests that patient-specific FE modeling may be useful for surgical planning of TTA to determine where the optimal location of a scar is in individuals. We further found that locating the surgical scar on the anterior aspect of

the residuum resulted in a higher concentration of stresses on the scar itself when compared to the inferior scars, which could indicate a risk for skin injuries or superficial PU for anterior scars.

One of the new features in this study is the inclusion of surgical scars in the TTA residuum models; this has never been considered before in the literature. The scar simulations were considerably different in internal tissue load values, and in locations of concentrated tissue loads, with respect to the no-scar reference case model (Table 3, Fig. 11). As mentioned above, the presence of the scars in the models substantially shifted and diverted internal tissue loads, particularly in the muscle flap, which demonstrates how important it is to include surgical scars in future FE modeling for improving the accuracy of representation of residual limbs.

Though we attempted to simulate the 3D biomechanical behavior of TTA residual limbs as accurately as possible, both in geometrical terms and in regard to nonlinear constitutive laws and properties for soft tissues, there are some limitations to the study. First, it is bounded to the analysis of standing, and cannot be used to deduce on internal tissue loads during gait. Some of the trends of data correlating the structure of the residuum (e.g., length of bones, tibial bevelment) to the internal state of loads could hold for the stance phase of gait, but this will require further modeling work that considers a dynamic system of musculoskeletal boundary condition forces. Another limitation is that the mechanical properties of muscle and fat tissues are extracted from healthy animal studies. Pathological changes to the constitutive properties of tissues that are specific to TTA, e.g., due to atrophy of denervated flaps which affects the microarchitecture of the tissue, might therefore influence the specific stress values obtained herein, but they are unlikely to affect the trends. Although several studies performed tissue indentation tests on different locations on the residual limbs of TTA patients,[22,47,48] these studies were all limited to measuring bulk soft tissue properties, and were unable to distinct between properties of different soft tissue layers (e.g., muscle and fat). Accordingly, for the muscle and fat components of our models, we adopted tissue properties from relevant animal studies (Table 2). Another limitation is that the plaster cast replica of the residuum used in the trial does not fully represent the prosthetic socket used by TTA patients. The commonly used TTA prosthetic socket is a patella-tendon-bearing (PTB) socket, which is indented in pressure-tolerant areas to allow shifting of loads away from the pressure-sensitive areas, e.g., the distal end of the residuum. This is further supported by the presence of a soft liner between the socket and skin of the residuum. The use of the unrectified cast may have resulted in some overestimation of tissue stresses. However, the assumption of an unrectified cast is consistent across the entire set of model variants, as the same cast geometry and cast properties were used in all simulation cases. The unrectified cast assumed in the modeling is therefore unlikely to interfere with the conclusions deduced from the comparison between the different simulation cases. Another limitation is the lack of representation for tendon tissues in our models but this is a reasonable assumption due to the custom surgical techniques for TTA. Surgeons are encouraged to perform TTA proximal to the lower third of the tibia to avoid incorporation of tendinous structures that are of poor circulation.[43] Last, although the distal end of the muscle flap is usually attached to the distal tibial end (myodesis) or to antagonist muscle groups (myoplasty), for the purpose of FE analysis, bone–muscle and muscle–fat interface nodes were assigned "tie" connections, so that no relative motion was allowed, in lack of experimental data to describe potential friction at these interfaces. Another factor potentially influencing relative motion between the bone–muscle and muscle–fat tissue layers, which was not considered in the modeling, is the fascia integrating these tissues.

It is not a straightforward task to compare 3D internal mechanical conditions in organs with different geometries, as in the TTA residuum studies herein. We introduced the stress analyses at the two VOI—BPL and FPL—to overcome these difficulties in a manner that allows data reduction and direct comparisons of strain/stress measures across the different anatomies. We intentionally refrained from simply comparing peak strain/stress values, due to numerical singularities that might occur around the distal tibial end, resulted from the artificial alteration of the geometry of the bones in some of the variant model configurations (Table 3). We therefore compared exposures to strains/stresses over VOI (the BPL and FPL), and in particular, percentages of volumes of these VOI that are subjected to stresses above a threshold of 2 kPa. Based on our preliminary work in preparation for this study, we believe that these outcome measures are less sensitive to focal abnormalities or numerical modeling artifacts.

In real-life situations there cannot be absolute separation between the surgical or physiological factors we studied herein. For example, it was found that the volume of the residuum is affected by muscle contraction. Specifically, muscle contraction in the TTA residual limb increased its volume by 3.5 and 5.8% with and without a silicone liner, respectively.[20] The coupling between volume change and muscle contraction was not taken into account in our analyses. A shorter tibial length was coupled in our analyses with a thicker muscular bulk, replacing the subtracted bone

(Fig. 2a). This relation, however, should be anatomically correct since for the shorter tibial lengths considered in this study the gastrocnemius muscle is naturally thicker, that is, because of the geometrical configuration, it envelopes the truncated bones closer to its belly, which is therefore contributing to a thicker cushioning.

Deep tissue injury is likely to be more common in dysvascular neuropathic patients whose pain mechanism is damaged, and therefore, as opposed to non-neuropathic amputees, they will not react to discomfort or pain during weight-bearing. On a broader aspect, potentially different implications of the present findings on traumatic and dysvascular patients are an important topic for future studies. The major difference between the trauma and dysvascular populations is obviously the quality of perfusion of their residuum, but specifically for patients with diabetes, there are also documented changes in stiffness of connective tissues, particularly skin, which are attributed to increased collagen fiber interlinks and fiber thickening.[9] Though neither perfusion of the residuum nor diabetes were the focus of this study, the stiffened skin characteristic of diabetic patients can be modeled using the present computational method.

CONCLUSIONS

Summarizing our conclusions, we found that stiff muscle flaps, e.g., spastic ones, endanger the TTA residual limb since the flap is overloaded by the tibial edge in a manner that could increase the likelihood for DTI. In the surgical environment, while a distal amputation is preferred by TTA surgeons for better gait stability and prosthetic control, the sharp edges of the truncated bones cause higher stresses and can potentially injure the muscle flap over time. A more inclined distal tibial bevelment causes higher concentrations of internal stresses and is therefore also theoretically increasing the risk for DTI. Consistent with reports in the medical literature,[13] our present computational data show that a calcified fibular osteophyte endangers the integrity and viability of soft tissues below the fibula by inducing focal stresses around the sharp bone tip. The osteophyte had a slight effect on the mechanical state of the residuum though. The location of the surgical scar affects the global flow of stresses from the tibia to the prosthetic socket, and an adherent scar, in particular, may draw a hazardous stress concentration toward it and toward the bone above it. From a research perspective, it is also important to consider surgical scars in a residual limb model, as they change the distribution of internal tissue loads with respect to a no-scar situation.

The results of this study can be compiled as guidelines for TTA surgeons, physical therapists, prosthetists, and the TTA patients themselves. Simple awareness of the biomechanical effects of each of these factors on internal tissue loads in the load-bearing residuum may already reduce hospitalization periods, clinical care costs, and enable more TTA patients to successfully use their prostheses and resume their daily life activities. Additionally, the present computational work may guide and focus epidemiological studies that attempt to identify risk factors for DTI or PU in the TTA population, thus saving on research cost, and allowing more efficient clinical follow-up trials. Last, the high variability in internal mechanical conditions in soft tissues of residual limbs, as demonstrated in this article (even though all the model variants were essentially based on the same anatomy), indicates the importance of patient-specific biomechanical modeling in TTA. The patient-specific modeling can be used for surgical planning as well as for assessing surgical outcomes of load transfer to soft tissues.

ACKNOWLEDGMENT

We appreciate the help of Mr. Shmulik Keidar (ADCOM Ltd., Givatayim, Israel) with technical issues related to the ABAQUS analyses.

REFERENCES

[1]Agam, L., and A. Gefen. Pressure ulcers and deep tissue injury: a bioengineering perspective. *J. Wound Care* 16:336–342, 2007.

[2]Ankrom, M. A., R. G. Bennett, S. Sprigle, D. Langemo, J. M. Black, D. R. Berlowitz, and C. H. Lyder. Pressure-related deep tissue injury under intact skin and the current pressure ulcer staging systems. *Adv. Skin Wound Care* 18:35–42, 2005.

[3]Avar, B. B., N. Hudyma, and M. Karakouzian. Porosity dependence of the elastic modulus of lithophysae-rich tuff: numerical and experimental investigations. *Int. J. Rock Mech. Min. Sci.* 40:919–928, 2003.

[4]Baum, B. S., B. L. Schnall, J. E. Tis, and J. S. Lipton. Correlation of residual limb length and gait parameters in amputees. *Injury* 39:728–733, 2008.

[5]Burgess, E. Amputations. *Surg. Clin. North. Am.* 63:749–770, 1983.

[6]Dou, P., X. Jia, S. Suo, R. Wang, and M. Zhang. Pressure distribution at the stump/socket interface in transtibial amputees during walking on stairs, slope and non-flat road. *Clin. Biomech.* 21:1067–1073, 2006.

[7]Dunn, M. G., F. H. Silver, and D. A. Swann. Mechanical analysis of hypertrophic scar tissue: structural basis for apparent increased rigidity. *J. Invest. Dermatol.* 84:9–13, 1985.

[8]Ertl, J. Uber amputationsstumpfe. *Chirurg* 20:218–224, 1949.
[9]Gefen, A. Plantar soft tissue loading under the medial metatarsals in the standing diabetic foot. *Med. Eng. Phys.* 25:491–499, 2003.
[10]Gefen, A., and E. Haberman. Viscoelastic properties of ovine adipose tissue covering the gluteus muscles. *J. Biomech. Eng.* 129:924–930, 2007.
[11]Gefen, A., B. Nierop, D. L. Bader, and C. W. Ooomens. Strain-time cell-death threshold for skeletal muscle in a tissue-engineered model system for deep tissue injury. *J. Biomech.* 41:2003–2012, 2008.
[12]Hendriks, F. M., D. Brokken, J. T. van Eemeren, C. W. Oomens, F. P. Baaijens, and J. B. Horsten. A numerical-experimental method to characterize the non-linear mechanical behaviour of human skin. *Skin Res. Technol.* 9:274–283, 2003.
[13]Henrot, P., J. Stines, F. Walter, N. Martinet, J. Paysant, and A. Blum. Imaging of the painful lower limb stump. *Radiographics* 20:S219–S235, 2000.
[14]Hoyt, K., T. Kneezel, B. Castaneda, and K. J. Parker. Quantitative sonoelastography for the in vivo assessment of skeletal muscle viscoelasticity. *Phys. Med. Biol.* 53:4063–4080, 2008.
[15]Kapp, S. Suspension systems for prostheses. *Clin. Orthop. Relat. Res.* 361:55–62, 1999.
[16]Kern, U., C. Martin, S. Scheicher, and H. Muller. Effects of botulinum toxin type B on stump pain and involuntary movements of the stump. *Am. J. Phys. Med. Rehabil.* 83:396–399, 2004.
[17]Lago, N., and X. Navarro. Evaluation of the long-term regenerative potential in an experimental nerve amputee model. *J. Peripher. Nerv. Syst.* 12:108–120, 2007.
[18]Laurent, A., F. Mistretta, D. Bottigioli, K. Dahel, C. Goujon, J. F. Nicolas, A. Hennino, and P. E. Laurent. Echographic measurement of skin thickness in adults by high frequency ultrasound to assess the appropriate microneedle length for intradermal delivery of vaccines. *Vaccine* 25:6423–6430, 2007.
[19]Lilja, M., P. Hoffmann, and T. Oberg. Morphological changes during early trans-tibial prosthetic fitting. *Prosthet. Orthot. Int.* 22:115–122, 1998.
[20]Lilja, M., S. Johansson, and T. Oberg. Relaxed versus activated stump muscles during casting for trans-tibial prostheses. *Prosthet. Orthot. Int.* 23:13–20, 1999.
[21]Linder-Ganz, E., S. Engleberg, M. Scheinowitz, and A. Gefen. Pressure-time cell death threshold for albino rat skeletal muscles as related to pressure sore biomechanics. *J. Biomech.* 39:2725–2732, 2006.
[22]Mak, A. F. T., G. H. W. Liu, and S. Y. Lee. Biomechanical assessment of below-knee residual limb tissue. *J. Rehabil. Res. Dev.* 31:188–198, 1994.
[23]Mattes, S. J., P. E. Martin, and T. D. Royer. Walking symmetry and energy cost in persons with unilateral transtibial amputations: matching prosthetic and intact limb inertial properties. *Arch. Phys. Med. Rehabil.* 81:561–568, 2000.
[24]Mooney, M. A theory of large elastic deformation. *J. Appl. Phys.* 11:582–592, 1940.
[25]Nadollek, H., S. Brauer, and R. Isles. Outcomes after trans-tibial amputation: the relationship between quiet stance ability, strength of hip abductor muscles and gait. *Physiother. Res. Int.* 7:203–214, 2002.
[26]Oomens, C. W., A. Stekelenburg, K. Ceelen, and D. Bader. A damage threshold for skeletal muscle under sustained mechanical loading. In: The Pathomechanics of Tissue Injury and Disease, and the Mechanophysiology of Healing, edited by A. Gefen. Kerala, India: Research Signpost, 2009, pp. 313–326. ISBN: 978-81-308-0314-2.
[27]Palevski, A., I. Glaitch, S. Portnoy, E. Linder-Ganz, and A. Gefen. Stress relaxation of porcine gluteus muscle subjected to sudden transverse deformation as related to pressure sore modeling. *J. Biomech. Eng.* 128:782–787, 2006.
[28]Peery, J. T., W. R. Ledoux, and G. K. Klute. Residual limb skin temperature in trans-tibial sockets. *J. Rehabil. Res. Dev.* 42:147–154, 2005.
[29]Pinzur, M. S., J. Beck, R. Himes, and J. Callaci. Distal tibiofibular bone-bridging in transtibial amputation. *J. Bone Joint Surg. Am.* 90:2682–2687, 2008.
[30]Pinzur, M. S., F. Gottschalk, M. A. Pinto, and D. G. Smith. Controversies in lower extremity amputation. *Instr. Course Lect.* 57:663–672, 2008.
[31]Pohjolainen, T. A clinical evaluation of stumps in lower limb amputees. *Prosthet. Orthot. Int.* 15:178–184, 1991.
[32]Portnoy, S., E. Atlas, and A. Gefen. Influence of bony prominence sharpness and underlying tissue stiffness on the susceptibility to pressure-related deep tissue injury: biomechanical computer model studies. *L'escarre* 36:4–7, 2007 (in French).
[33]Portnoy, S., G. Yarnitzky, Z. Yizhar, A. Kristal, U. Oppenheim, I. Siev-Ner, and A. Gefen. Real-time patient-specific finite element analysis of internal stresses in the soft tissues of a residual limb: a new tool for prosthetic fitting. *Ann. Biomed. Eng.* 35:120–135, 2007.
[34]Portnoy, S., Z. Yizhar, N. Shabshin, Y. Itzchak, A. Kristal, Y. Dotan-Marom, I. Siev-Ner, and A. Gefen. Internal mechanical conditions in the soft tissues of a residual limb of a trans-tibial amputee. *J. Biomech.* 41:1897–1909, 2008.
[35]Randon, C., J. Deroose, and F. Vermassen. How to perform a below-knee amputation. *Acta Chir. Belg.* 103:238–240, 2003.
[36]Rommers, G. M., L. D. Vos, L. Klein, J. W. Groothoff, and W. H. Eisma. A study of technical changes to lower limb prostheses after initial fitting. *Prosthet. Orthot. Int.* 24:28–38, 2000.
[37]Salawu, A., C. Middleton, A. Gilbertson, K. Kodavali, and V. Neumann. Stump ulcers and continued prosthetic limb use. *Prosthet. Orthot. Int.* 30:279–285, 2006.
[38]Sanders, J. E., J. R. Fergason, S. G. Zachariah, and A. K. Jacobsen. Interface pressure and shear stress changes with amputee weight loss: case studies from two trans-tibial amputee subjects. *Prosthet. Orthot. Int.* 26:243–250, 2002.
[39]Sanders, J. E., J. M. Greve, S. B. Mitchell, and S. G. Zachariah. Material properties of commonly-used interface materials and their static coefficients of friction with skin and socks. *J. Rehabil. Res. Dev.* 35:161–176, 1998.
[40]Sanders, J. E., S. G. Zachariah, A. B. Baker, J. M. Greve, and C. Clinton. Effects of changes in cadence, prosthetic componentry, and time on interface pressures and shear stresses of three trans-tibial amputees. *Clin. Biomech.* 15:684–694, 2000.
[41]Sanders, J. E., S. G. Zachariah, A. K. Jacobson, and J. R. Fergason. Changes in interface pressures and shear stresses over time on trans-tibial amputee subjects ambulating with prosthetic limbs: comparison of diurnal and six-month differences. *J. Biomech.* 38:1566–1573, 2005.
[42]Schmalz, T., S. Blumentritt, and R. Jarasch. Energy expenditure and biomechanical characteristics of lower limb amputee gait: the influence of prosthetic alignment and different prosthetic components. *Gait Posture* 16:255–263, 2002.

[43]Schwartz, S., F. Spencer, A. Galloway, G. Shires, J. Daly, and J. Fischer. Principles of Surgery (7th ed.). New York: McGraw-Hill, pp. 991–999, 1998.

[44]Silver-Thorn, M. B. Prediction and experimental verification of residual limb/prosthetic socket interface pressures for below-knee amputees. PhD Thesis, Department of Biomedical Engineering, Northwestern University, Chicago, IL, USA, 1991.

[45]Smith, K. E., P. K. Commean, and M. W. Vannier. Residual limb shape change: three-dimensional CT scan measurement and depiction in vivo. *Radiology* 200:843–850, 1996.

[46]Smith, D. G., L. V. McFarland, B. J. Sangeorzan, G. E. Reiber, and J. M. Czeniecki. Postoperative dressing and management strategies for trans-tibial amputations: a critical review. *J. Rehabil. Res. Dev.* 40:213–224, 2003.

[47]Tonuk, E., and M. B. Silver-Thorn. Nonlinear viscoelastic material property estimation of lower extremity residual limb tissues. *J. Biomech. Eng.* 126:289–300, 2004.

[48]Vannah, W. M., D. M. Drvaric, J. A. Hastings, J. A. Stand, 3rd, and D. M. Harning. A method of residual limb stiffness distribution measurement. *J. Rehabil. Res. Dev.* 36: 1–7, 1999.

[49]Wilson, A. B. History of amputation surgery and prosthetics. In: Atlas of Limb Prosthetics: Surgery and Prosthetic Principles, edited by J. H. Bowker and J. W. Michael. American Academy of Orthopedic Surgeons. St. Louis, MO: Mosby, 1981.

[50]Zhang, M., and C. Roberts. Comparison of computational analysis with clinical measurement of stresses on below-knee residual limb in a prosthetic socket. *Med. Eng. Phys.* 22:607–612, 2000.